Astronomy & Astrophysics manuscript no. sori˙lori˙final
May 19, 2008
© ESO 2008

arXiv:0805.2914v1 [astro-ph] 19 May 2008

FLAMES spectroscopy of low-mass stars in the young clusters σ Ori and λ Ori*

G. G. Sacco[1,2], E. Franciosini[1], S. Randich[4], and R. Pallavicini[1,3]

[1] INAF, Osservatorio Astronomico di Palermo, Piazza del Parlamento, 1, 90134 Palermo, Italy

[2] Consorzio COMETA, Via S. Sofia, 64, 95123 Catania, Italy
e-mail: sacco@astropa.inaf.it

[3] INAF, Headquarters, Viale del Parco Mellini 84, 00136 Roma, Italy

[4] INAF, Osservatorio Astrofisico di Arcetri, Largo E. Fermi, 50125 Firenze, Italy

Received 12 November 2007/ accepted .....

ABSTRACT

Aims. We performed a detailed membership selection and studied the accretion properties of low-mass stars in the two apparently very similar young (1-10 Myr) clusters σ Ori and λ Ori.
Methods. We observed 98 and 49 low-mass ($0.2 - 1.0 M_\odot$) stars in σ Ori and λ Ori respectively, using the multi-object optical spectrograph FLAMES at the VLT, with the high-resolution ($R \sim$17,000) HR15N grating (6470−6790 Å). We used radial velocities, Li and Hα to establish cluster membership and Hα and other optical emission lines to analyze the accretion properties of members.
Results. We identified 65 and 45 members of the σ Ori and λ Ori clusters, respectively and discovered 16 new candidate binary systems. We also measured rotational broadening for 20 stars and estimated the mass accretion rates in 25 stars of the σ Ori cluster, finding values between 10^{-11} and $10^{-7.7} M_\odot$ yr^{-1} and in 4 stars of the λ Ori cluster, finding values between 10^{-11} and $10^{-10.1} M_\odot$ yr^{-1}. Comparing our results with the infrared photometry obtained by the *Spitzer* satellite, we find that the fraction of stars with disks and the fraction of active disks is larger in the σ Ori cluster (52±9% and 78±16%) than in λ Ori (28±8% and 40±20%).
Conclusions. The different disk and accretion properties of the two clusters could be due either to the effect of the high-mass stars and the supernova explosion in the λ Ori cluster or to different ages of the cluster populations. Further observations are required to draw a definitive conclusion.

Key words. Stars: formation – Stars: pre-main sequence – Stars: late-type – open clusters and associations: individual: σ Ori, λ Ori

1. Introduction

The time evolution of accretion properties and disk dissipation mechanisms in young stars are two of the main open issues in the star formation theory. The analysis of the accretion properties of the stellar populations belonging to young clusters, using high-resolution ($R \sim$20,000) spectroscopy, is a powerful tool to investigate these questions. Among young clusters, σ Ori and λ Ori are two of the richest clusters near the Sun in the age range (1−10 Myr) during which young stars lose their circumstellar disk and stop accreting material from it (Hartmann et al. 1998; Haisch et al. 2001; Sicilia-Aguilar et al. 2005, 2006).

The σ Ori cluster was discovered by the *ROSAT* satellite (Wolk 1996; Walter et al. 1997) around the O9.5 V binary star σ Orionis AB (distance 352^{+166}_{-85} pc, Perryman et al. 1997). Because of its proximity and very low reddening (Oliveira et al. 2004), during the last decade σ Ori has become one of the best studied young clusters. Its low-mass and substellar population, extending down to planetary-mass objects, has been extensively observed by photometry and low-resolution spectroscopy, both in infrared and optical bands (Zapatero Osorio et al. 2000; Béjar et al. 2001; Zapatero Osorio et al. 2002; Barrado y Navascués et al. 2003; Scholz & Eislöffel 2004; Sherry et al. 2004; Béjar et al. 2004; Burningham et al. 2005; Kenyon et al. 2005; Caballero et al. 2007), while its high-mass stellar content has been studied by Caballero (2007). The estimated median age of the cluster ranges from 1 to 8 Myr, depending on the assumed distance and measurement method adopted by different authors. Using measurements of tangential and radial velocities, Jeffries et al. (2006) and Caballero (2007) argued that, in the same region of the σ Ori cluster, there is a sparser, kinematically separate young stellar population belonging to the Orion OB1b association. Zapatero Osorio et al. (2002), using low-resolution spectroscopy of a sample of 27 low-mass and substellar objects, estimated a fraction of about 30−40% of classical T Tauri stars (CTTSs), while the fraction of circumstellar disks (33±6%) was first determined by Oliveira et al. (2004, 2006), using infrared photometric data in the *K* and *L* bands. Recently, Hernández et al. (2007) used a near-infrared survey carried out by the *Spitzer* satellite to investigate the disk properties of 336 candidate members, finding that 34% of them harbor a circumstellar disk (27% having thick disks and 7% having evolved optically thin disks). Moreover, they found that the total fraction of stars with disks decreases with increasing mass from 36% (31% with thick disks) for low-mass T Tauri stars to 15% (4% with

Send offprint requests to: G.G. Sacco, e-mail: sacco@astropa.inaf.it

⋆ Based on Data collected at the ESO Very Large Telescope, Paranal Observatory, Chile [programs 074.D-0136(A) and 076.C-0125(A)]

thick disks) for Herbig Ae/Be stars. Finally, the X-ray properties of high-mass and low-mass cluster members have been studied by Sanz-Forcada et al. (2004) and Franciosini et al. (2006) using the *XMM-Newton* satellite.

λ Orionis is an O8 III star (distance 400 pc, Murdin & Penston 1977) which excites the HII region S264, delimited by a dust ring with a diameter of 9° discovered by the *IRAS* satellite (Zhang et al. 1989). The cluster, distributed over an area of 1 square degree around the O8 star, was discovered by Gomez & Lada (1998) together with two clusters located in the nearby clouds B30 and B35, by analyzing the spatial correlation among the Hα sources discovered by Duerr et al. (1982). Dolan & Mathieu (1999), using medium-resolution spectroscopy, selected 72 members brighter than $R = 16$ around λ Orionis and found that the fraction of CTTSs (7%) belonging to the cluster is very low if compared to other clusters and star-forming regions in the same age range (1−10 Myr). Dolan & Mathieu (2001, 2002) extended this analysis to the whole region and suggested that the star formation process started 8−10 Myr ago, with an accelerating star-formation rate, and stopped 1−2 Myr ago after a supernova explosion, which shredded the central cloud and formed the current gas ring. They also suggested that, before the supernova explosion, the cluster was still bound to its natal cloud, therefore the young stars closer to the central OB stars, including also the supernova progenitor, lost their circumstellar disks due to photoevaporation by the far-ultraviolet emission from the high mass stars. Barrado y Navascués et al. (2004) selected 170 candidate members through deep optical photometry and performed low-resolution spectroscopy of 33 very low-mass and substellar objects. The properties of circumstellar disks have been studied by Barrado y Navascués et al. (2007) by means of the *Spitzer* satellite. They found that the total fraction of members with disks (both thick and evolved optically thin disks) is 31%, but the fraction of stars with a thick disk is only 14%. They also found that the distribution of Class II stars is inhomogeneous, namely, most of them are located in a filament that goes from λ Orionis to the B35 cloud. Moreover, since several Class II stars are located near the cluster center, they argued that high-mass stars and the supernova explosion had no effect on the circumstellar disks.

Although the two clusters have been extensively observed during the last decade, only few spectroscopic data at a resolution equal to or higher than $R = 10,000 - 15,000$ are available and, especially for the σ Ori cluster, most of the cluster members have been selected by means of photometry only. Therefore, the catalogues of members of both clusters are likely contaminated by foreground field stars or young stellar objects belonging to different populations, and the accretion properties of the known members are poorly determined.

We performed high-resolution spectroscopy of two large samples of stars in the σ Ori and λ Ori clusters, using FLAMES at the VLT (Pasquini et al. 2002), in order to select new high-probability cluster members, to identify CTTSs using Hα emission and other accretion indicators and to measure mass accretion rates (MARs). Moreover, the comparison between the "twin" clusters σ Ori and λ Ori is a powerful tool to investigate the origin of the presumed lack of CTTSs in the λ Ori cluster. In Sacco et al. (2007) we reported a first important result for the σ Ori cluster, obtained from the analysis of these data, namely, the discovery of three Li-depleted stars, with isochronal and nuclear ages greater than 10−15 Myr. In this paper, we focus on the other results obtained by these data.

The paper is organized as follow: in Sect. 2 we describe target selection, observations and data analysis; results are presented in Sect. 3 and discussed in Sect. 4, where we also perform a comparison with the infrared data obtained by the *Spitzer* satellite. Conclusions are summarized in Sect. 5.

2. Observations and data analysis

2.1. Target selection

We selected sources in the σ Ori and λ Ori cluster regions in the spectral range K6−M5, which, for a 5 Myr cluster at a distance of about 400 pc, corresponds to the magnitude ranges $13< R <18$ and $11< J <15$. All selected sources, except 4 objects without optical photometry, are plotted in Fig. 1, where different symbols indicate the membership information available before this work.

For the σ Ori cluster, targets were selected using optical, infrared and X-ray data. Optical and infrared data were retrieved from the literature (Wolk 1996; Zapatero Osorio et al. 2002; Sherry et al. 2004; Kenyon et al. 2005) and the 2MASS (2 Micron All Sky Survey) catalogue (Skrutskie et al. 2006). X-ray data were retrieved from Franciosini et al. (2006). We selected a total of 98 objects; of these, 18 are probable members on the basis of low-resolution spectroscopy, 66 are candidate members on the basis of optical and/or infrared photometry compatible with an age $\lesssim$10 Myr (taking also into account the error on distance) and the remaining 14 objects appear to be non-members based on photometry, but have no spectroscopic information. Of the 98 targets, 53 were also detected in X-rays.

In the λ Ori cluster we observed 49 sources, included in the catalogues by Dolan & Mathieu (1999) (5 objects), by Barrado y Navascués et al. (2004) (34 objects) or by both (10 objects). The stars included in the Dolan & Mathieu (1999) catalogue are probable members on the basis of medium-resolution spectroscopy, while the other stars are candidate members based on photometric selection, with 3 objects confirmed as members also by low-resolution spectroscopy.

The sources selected in the σ Ori and λ Ori clusters are listed in Table 1 and in Table 2, respectively. Optical and infrared magnitudes are retrieved from the literature; spectral types for 18 stars are from previous spectroscopic studies (Zapatero Osorio et al. 2002; Barrado y Navascués et al. 2004), while for the other stars they have been derived from the $R - I$ color, using the scale of Kenyon & Hartmann (1995) interpolated for each half subtype. We did not derive spectral types from our data, because the spectral range covered by our spectra does not include enough spectral features for the classification, and because veiling affecting accreting objects prevents the use of spectroscopic indices based on flux ratios. For the stars with a spectroscopic classification already performed by other authors, we checked that the discrepancy between photometric and spectroscopic spectral type is $\leq$1 subtype for 12 stars, between 1 and 2 subtypes for 4 stars and of 2.5 subtypes in 2 cases (S07 and L44).

We cross-correlated our list of targets with the catalogues of stars observed by the *Spitzer* satellite, published by Hernández et al. (2007) for σ Ori and by Barrado y Navascués et al. (2007) for λ Ori. We have 83 sources in common with the Hernández et al. (2007) catalogues, 78 with the catalogue of probable members and 5 with the catalogue of uncertain members, and 44 sources in common with the Barrado y Navascués et al. (2007) catalogue. Taking into account the classification based on the slope α of the spectral energy distributions in the 3.6−8.0 μm spectral range,

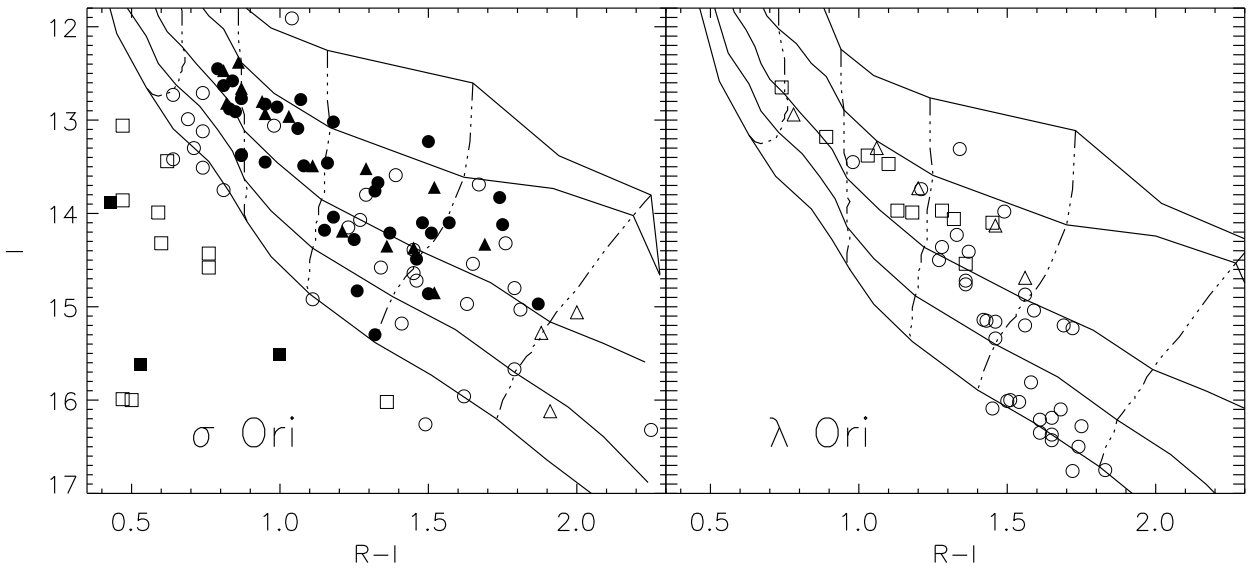

Fig. 1. Color-magnitude diagrams of the selected objects in the σ Ori (left panel) and λ Ori (right panel) clusters. In the left panel, triangles represent the probable members on the basis of low-resolution spectroscopy, circles represent the candidate members on the basis of photometry and squares represent the non-members on the basis of photometry; filled symbols mark sources with an X-ray counterpart. In the right panel, triangles represent the sources included only in the Dolan & Mathieu (1999) catalogue, circles represent the sources included only in the Barrado y Navascués et al. (2004) catalogue and squares represent the sources included in both catalogues. Continuous and dotted lines are, respectively, isochrones at 1, 2, 5, 10 and 20 Myr and tracks at 0.2, 0.3, 0.4, 0.6, 1.0 $M_{\odot}$ from the Siess et al. (2000) models, using the Kenyon & Hartmann (1995) table for the conversion of colors and magnitudes into temperatures and luminosities. Isochrones and tracks are corrected for the distance modulus (7.72 and 8.01 for σ Ori and λ Ori, respectively) and in the case of λ Ori also for reddening, considering a color excess $E(B-V) = 0.12$ (Diplas & Savage 1994) and using the Munari & Carraro (1996) transformation laws; for the σ Ori cluster, as discussed by Oliveira et al. (2004), reddening is negligible.

in the σ Ori cluster sample there are 34 stars harboring a circumstellar disk ($\alpha > -2.56$) and 49 diskless stars, while in the λ Ori sample there are 11 stars with a circumstellar disk and 33 diskless stars.

2.2. Observations and data reduction

Observations were carried out using the fiber-fed multi-object spectrograph FLAMES (Fiber Large Array Multi Element Spectrograph), mounted on the UT2 telescope at the VLT (Pasquini et al. 2002) and operated in the MEDUSA mode (132 fibers, each with an aperture of 1.2 arcsec on the sky). We used for both clusters the high resolution HR15N grating (6470−6790 Å, spectral resolution R =17,000 and nominal dispersion 0.1 Å pixel^{-1}), which includes the lithium line at 6708 Å, the Hα line (6563 Å) and other emission lines indicative of accretion and outflow phenomena (NII at 6583 Å, HeI at 6678 Åand SII at 6716 and 6731 Å). For λ Ori only, we used also the HR21 grating (8480−9000 Å, spectral resolution R =16,200 and nominal dispersion 0.13 Å pixel^{-1}), which includes the Ca II infrared triplet, but, since no star in our sample shows signs of Ca II emission due to accretion phenomena (see Sect. 3.3), these spectra have been used only for the measurement of the radial velocity (RV). For both clusters the FLAMES field of view (diameter 25′) was centered around the high-mass central star which gives the name to the cluster (RA=5h 38m 48.9s, DEC= -2d 34m 22s and RA=5h 35m 06.5s, DEC= 9d 54m 0.0s, Equinox J2000, for σ Ori and λ Ori, respectively).

Observations were performed in service mode and were divided into separate runs of 1 hour duration each, including instrument overheads. The σ Ori cluster was observed in 6 runs in October and December 2004, while λ Ori was observed in 8 runs in October and November 2005. The observation log is reported in Table 3.

Table 3. Observation log.

cluster	setup	exposure time[a] (m)	run dates
σ Ori	HR15N	43.2	2004-10-01
σ Ori	HR15N	40.3	2004-12-01
σ Ori	HR15N	43.2	2004-12-02
σ Ori	HR15N	43.2	2004-12-03
σ Ori	HR15N	43.2	2004-12-04
σ Ori	HR15N	43.2	2004-12-09
λ Ori	HR15N	46.0	2005-10-15
λ Ori	HR15N	46.0	2005-10-16
λ Ori	HR15N	46.0	2005-10-17
λ Ori	HR15N	46.0	2005-11-10
λ Ori	HR21	46.0	2005-11-12
λ Ori	HR21	46.0	2005-11-12
λ Ori	HR21	46.0	2005-11-12
λ Ori	HR21	46.0	2005-11-23

a: Excluding instrument overheads

Data reduction was performed using the GIRAFFE girBLDRS pipeline vers. 1.12, following the standard steps (Blecha & Simond 2004), which include bias subtraction, division by a normalized flat-field, correction for the differences in the fiber transmission, and wavelength calibration using a dispersion solution from a Thorium-Argon arc lamp. The spectra

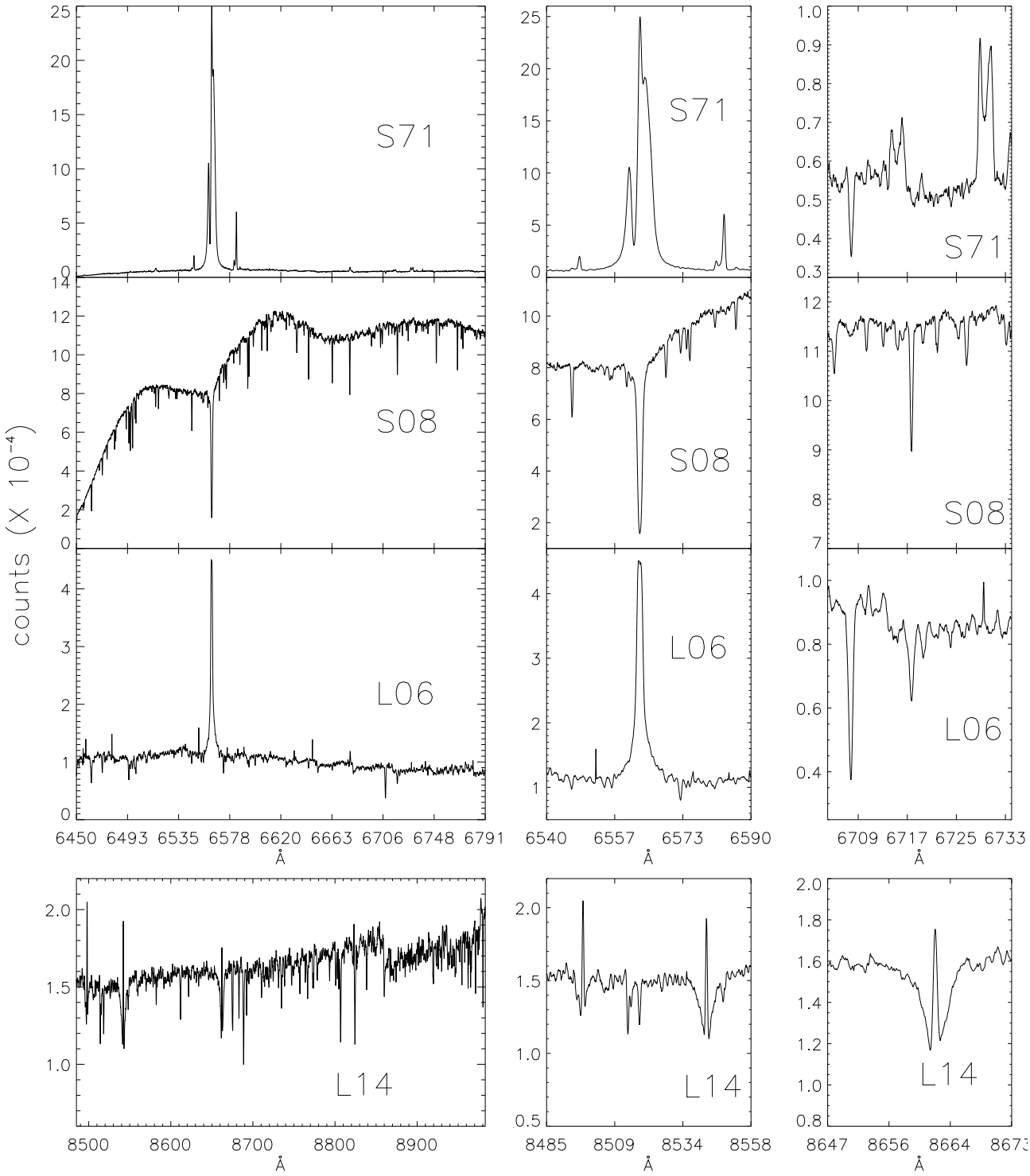

Fig. 2. Spectra of 4 stars of the sample. The three upper rows show spectra obtained with the HR15 grating: in the left panels we show the whole spectral range, while the middle and right panels show the range around the Hα and the Li line, respectively. For star S71, in the right panel the SII doublet at 6716 and 6731 Å can also be seen. The bottom row show a spectrum obtained with the HR21 grating: the whole spectrum is shown in the left panel, while the middle and right panels show the range around the CaII triplet.

processed by the pipeline are not corrected for instrumental response and sky background, but, except for the RVs, all measurements were performed on the sum of the spectra recorded in the different runs, after subtracting a sky background spectrum. The sky background was calculated independently for each observing run, using a set of fibers homogeneously distributed over the field (10 for σ Ori and 20 for λ Ori). For each run, we averaged a subsample of sky spectra without intense spikes. To increase the signal-to-noise ratio (S/N) for line measurements, we then summed together, for each source, the spectra from the different runs. The S/N of the summed spectra ranges from ∼10 for stars

with I ∼16, to ∼90 for stars with I ∼14 and to ∼170 for stars with I ∼12. Some examples of stellar spectra are shown in Fig. 2.

2.3. Radial velocities

We measured, independently, the RVs in each observing run, with the aim of identifying cluster members and selecting candidate binary systems. RVs were measured by Fourier cross-correlation (Tonry & Davis 1979), using the IRAF[1] task FXCOR. In brief, all the spectra were cross-correlated with one template spectrum chosen among the stars belonging to the observed sample (stars S07 and S56 for σ Ori and L04 and L17 for λ Ori). Specifically, stars S07 and L04 have been used only for earlier type stars, and stars S56 and L17 for the others. The template spectra have been selected on the basis of their spectral type (K and M), high S/N (40−200), low rotational velocities (line full width at half maximum <0.6 Å) and because they do not show any accretion signatures. However, the Hα, other emission lines and telluric lines have been excluded from the cross-correlated spectral range. In order to determine the RVs relative to the solar system, we measured the centroid shifts of a selected group of lines in the template spectra, using the IRAF task RVIDLINES.

For the stars with a single main peak in the cross-correlation function and with all the RVs in agreement within 2σ, we computed a mean RV as the weighted average of the different measurements. The measured RVs are given in Tables 1 and 2 for the σ Ori and the λ Ori cluster, respectively. The other stars, classified as candidate binaries, are discussed in Sect. 3.1.

2.4. Rotational velocities

We were able to measure the rotational velocities (vsin i) of 20 stars and to estimate a vsin i upper limits of all the remaining members identified in the two clusters (see Sect. 3.2) and not classified as binary systems (see Sect. 3.1).

Rotational velocities were measured by cross-correlating the spectra of each star with the spectra of the stars L04 (for stars with spectral-type earlier than M2) and S88 (for stars with later spectral-type stars), using the IRAF task FXCOR. Both stars used as templates show very narrow lines (full width half maximum –FWHM–<0.540 Å) and have S/N >20. Specifically, vsin i is related to the FWHM of the Gaussian which better describes the peak of the cross-correlation function by a calibration function. In order to derive the calibration function, we first cross-correlated each template spectra with itself artificially broadened at different velocities using the rotational profile of Gray (1992); then, we fitted the relation between the values of FWHM and the rotational velocities with a third order polynomial.

Errors on vsin i depend on the uncertainties in the cross-correlation process between the template and the stars spectra; these have been estimated by varying the Gaussian fit parameters within reasonable ranges. Moreover, taking into account the features of the template spectra and the uncertainties in our procedure, we concluded that the lowest measurable rotational velocity is ∼17 km/s, which corresponds to a line broadening equal to the instrumental broadening.

Inferred vsin i and upper limits are listed in Col. 12 in Tables 1 and 2.

[1] IRAF is distributed by the National Optical Astronomy Observatory, which is operated by the Association of Universities for Research in Astronomy, Inc.,under contract to the National Science Foundation.

2.5. Pseudo equivalent width of absorption and emission lines

We measured the equivalent width of the Li line at 6708 Å and of 5 emission lines (Hα, NII at 6583 Å, HeI at 6678 Å and SII at 6716 and 6731 Å), using the IRAF task SPLOT, by integrating the area under the continuum level. For the lithium line, we integrated all the spectra over the same range (6705.8−6709.5 Å at a rest reference frame). For the emission lines, we integrated on a spectral range different from star to star, because accretion lines can be shifted or broadened, depending on the velocity of the outflowing or accreting material. The lithium line measurements are reported in Tables 1 and 2, while the emission line measurements are reported in Tables 4 and 5, for the σ Ori and the λ Ori clusters, respectively. Due to the presence of molecular bands, which strongly affect the spectrum of late-type stars, the EWs are measured with respect to a false continuum. To remark this point, in the rest of the paper we refer to these measurements as pseudo-equivalent widths (pEWs). We did not measure any pEW of the double-lined binaries and of the star L48, because in the former case we could not separate the contributions of the different components of the binary system, while in the latter the S/N is too low to estimate the continuum level after the sky subtraction.

For the Li and Hα lines, we derived the pEWs as the average of 3 independent measurements carried out by selecting a minimum, a maximum and a median continuum level. Errors have been computed as the half-difference between the maximum and minimum of the 3 measurements. We measured the Li pEW by integrating over the 6705.8−6709.5 Å range even in the case where the presence of the Li line was not evident. In these cases, the line pEW is always below 150 mÅ, while in the other cases the pEW is always higher than 250 mÅ except for the star S55, which, as discussed in Sacco et al. (2007), has started to deplete its photospheric lithium.

For the pEWs of other emission lines, we took a single measurement and, whenever the presence of the line was not evident in the spectrum, we estimated an upper limit on the basis of the faintest measurable lines observable in the same spectral range.

2.6. Hα width at 10% of the peak

We measured the width of the Hα line at 10% of the peak in order to discriminate between accreting and non-accreting objects and to derive the mass accretion rates (MARs), using the following relationship:

$$\log(\dot{M}_{acc}) = -12.89(\pm0.3) + 9.7(\pm0.7) \times 10^{-3} H\alpha_{10\%} \quad (1)$$

where H$\alpha_{10\%}$ is the Hα width at 10% of the peak in km s^{-1} and $\dot{M}_{acc}$ is the MAR in $M_{\odot}$ yr^{-1}. This relationship was empirically derived by Natta et al. (2004), using independent measurements of MARs and Hα widths in a sample of stars spanning a range of masses from about 0.04 to 0.8 $M_{\odot}$. According to Natta et al. (2004), this relationship holds for H$\alpha_{10\%} \geq$ 200 km s^{-1}, but other authors (White & Basri 2003) used the more conservative threshold of 270 km s^{-1}.

The Hα widths of cluster members and MARs of the stars harboring a disk are reported in Tables 4 and 5 for σ Ori and λ Ori, respectively. Errors on the Hα widths depend on the uncertainties in the continuum flux, which affect the determination of the 10% level, while the errors on the MARs depend both on the errors on the Hα width and on the uncertainties on the parameters included in Eq. (1). For binary systems the Hα widths

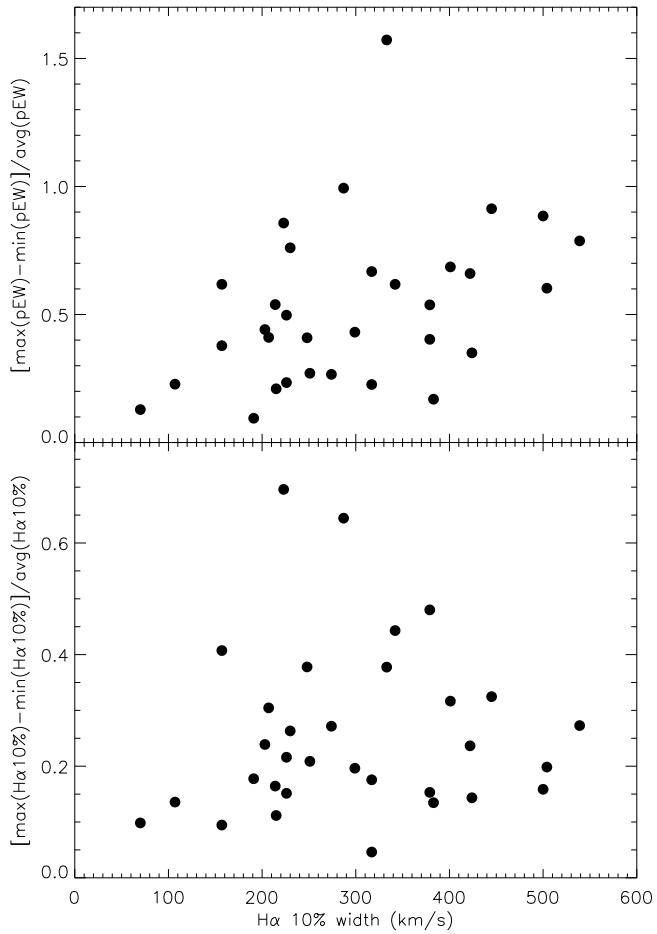

Fig. 3. Hα variability of the CTTSs as a function of the Hα width. The upper and bottom panels show, respectively, the variability of the pEWs and of the Hα width at 10% of the peak.

have been considered undetermined in order to avoid systematic errors related to the presence of two spectra shifted at different velocities.

2.7. Hα variability

We investigated the variability of the Hα pEWs for all the stars, and of the Hα width at 10% of the peak for the CTTSs, by comparing the measurements performed in each individual observing run. Among the WTTSs the median variability ((max(pEW)-min(pEW))/average(pEW)) ranges between 0.1 and 1.9, with a median value of 0.37, but it is larger than 1.0 only for three stars (S28, L06, L36). For the latter stars, the variation is observed only in a single run, suggesting that it was probably recorded during a flaring event.

The variability of the pEWs and of the 10% widths for the CTTSs is plotted in Fig. 3 as a function of the 10% widths measured on the summed spectra. As shown in the figure, we do not find evidence for any correlation between the two measurements of variability and the 10% width, which, as explained in the previous section, is correlated with the mass accretion rate. The median value, the mean and the standard deviation of the variability of the pEWs are 0.50, 0.53 and 0.31, respectively, while the median, mean and standard deviation of the 10% widths are 0.22, 0.26 and 0.15, respectively. In 5 cases (S05, S33, S65, S98 and L34) for the pEWs and in 4 cases (S12, S65, S69 and L34) for the 10% widths, the variations differ by more than 3σ from the mean of the sample. In the case of the star S23, which is not included in Fig. 3, we find a variability of the Hα pEW $\geq$4, because the line is composed of both absorption and emission features, and the pEW is positive in some runs and negative in others.

Moreover, the intrinsic variability is in most cases higher than the errors on the measurements of the Hα pEWs and 10% widths, which are of the order of 10%, as can be seen from Tables 4 and 5.

3. Results

3.1. Binaries

We found 11 stars in σ Ori and 5 in λ Ori for which at least 2 of the measured RVs differ by more than 2σ, and therefore we classified them as candidate binaries. The measured RVs in each run are given in Tables 6 and 7. Specifically, in the σ Ori sample, for 6 binaries all the RVs are not in agreement among each other. Of these, 5 stars show a cross-correlation function with two distinct peaks, corresponding to the RVs of both components of the binary system. The RVs as a function of time for these 6 binaries are plotted in Fig. 4, and show a well-defined sinusoidal trend. We have performed a least-squares fit to the RV curves using a sine function; in the case of double-lined binaries, both curves were fitted simultaneously.

The binary system parameters derived from the fits with their 1σ uncertainties are given in Table 8. For the other 5 candidate binaries in σ Ori, only the RV measured in October 2004 does not agree with the other 5 RVs measured in December 2004, that are compatible within the errors. A careful check of the October spectra did not evidence any reduction or analysis problem, therefore we believe that the observed discrepancy is real. These stars might therefore be binaries with a period of some months, for which RV variations cannot be detected in the observations taken in December, which are distributed over a period shorter than 10 days. Further RV measurements are required to confirm their nature.

In the λ Ori cluster, we found one star with two distinct peaks in the cross-correlation function, for which however we cannot obtain a fit to the RV data, and 4 stars with at least two of the measured RVs differing by more than twice the error bar.

For the selection of members from RVs, we used the derived center of mass velocities for the binary systems listed in Table 8. For the other binaries, the system velocities cannot be determined, and will therefore not be used for their membership determination.

3.2. Membership

To determine cluster membership we used three independent criteria, based on the RV distribution, the pEW of the Li absorption line, and the presence of the Hα line in emission.

In Fig. 5 we show the RV distributions for the observed stars in σ Ori and λ Ori, excluding the 10 probable binaries (5 for each cluster) for which the velocity of the center of mass is undetermined. The two distributions have been fitted with the weighted sum of two Gaussian functions (shown in Fig. 5 with dashed curves), one describing the velocity distribution of the cluster members and the other describing the velocity distribution of the field stars. For σ Ori the cluster distribution is centered at V_C = 30.93 km s^{-1}, with a standard deviation σ_C = 0.92 km s^{-1}, while for the field star distribution we find

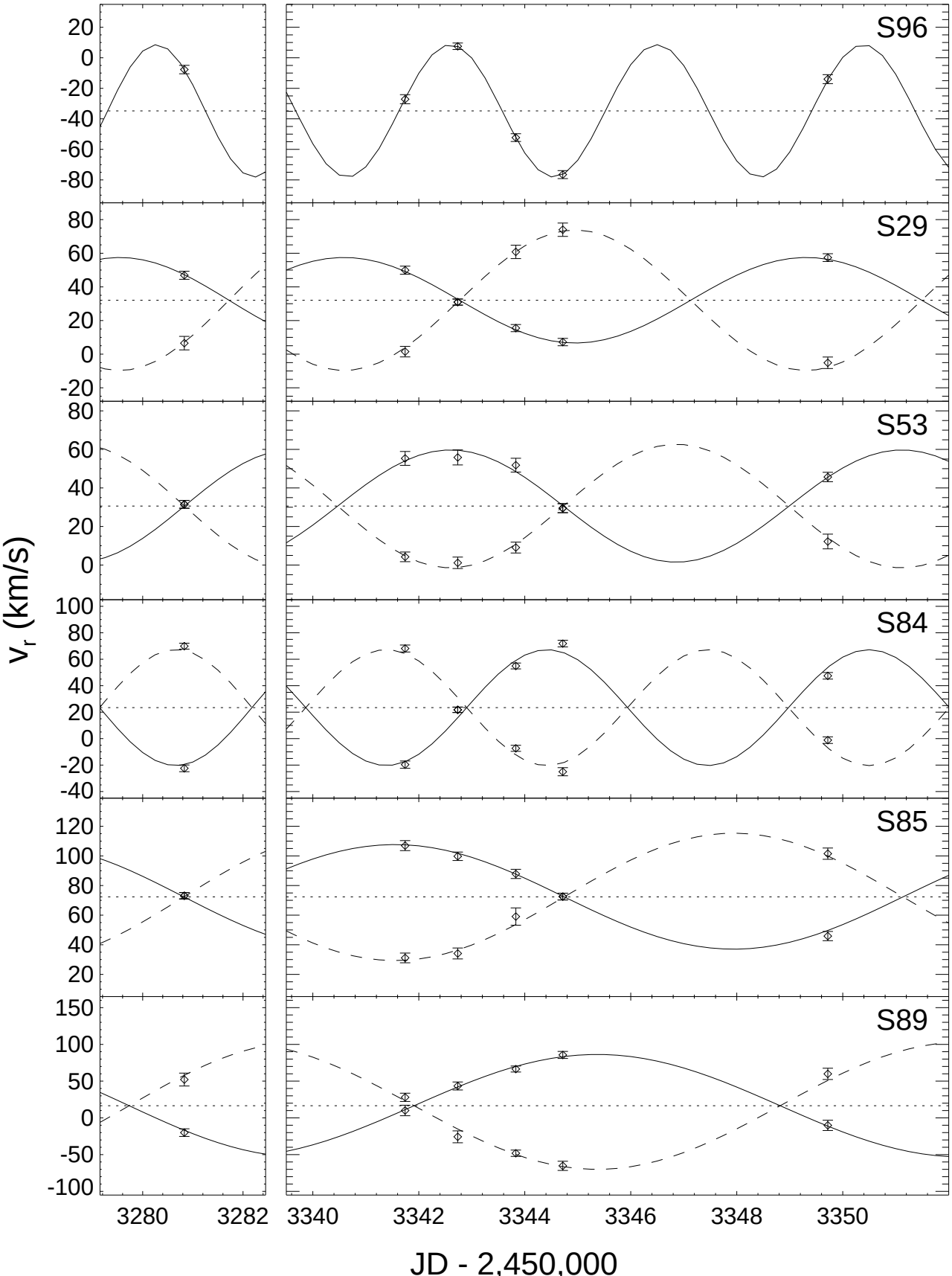

Fig. 4. Velocity vs. time for the 6 binary systems reported in Table 8. In the left and right panels we show the values obtained from the runs performed in October and December, respectively. The continuous and dotted curves show the sine functions which fit the data.

Table 6. Radial velocities of the candidate binary systems identified in the σ Ori cluster sample.

	JD-2453000.00					
	280.82	341.73	342.73	343.82	344.71	349.71
ID	RV (km/s)	RV (km/s)	RV (km/s)	RV (km/s)	RV (km/s)	RV (km/s)
S04	17.83 ± 4.81	33.10 ± 3.01	34.19 ± 6.17	32.21 ± 4.64	27.55 ± 6.40	34.94 ± 4.57
S26	27.95 ± 3.38	43.72 ± 2.90	43.07 ± 3.35	44.88 ± 3.34	45.25 ± 3.18	44.32 ± 4.01
S29a	6.56 ± 4.03	1.51 ± 3.13	30.97 ± 1.82	60.81 ± 3.99	73.99 ± 3.96	-5.13 ± 3.42
S29b	46.91 ± 2.40	49.93 ± 2.41	30.97 ± 1.82	15.51± 2.11	7.20 ± 2.18	57.42 ± 2.32
S43	39.17 ± 1.41	21.10 ± 1.59	18.60 ± 1.67	20.96 ± 1.53	20.13 ± 1.62	22.40 ± 1.30
S50	11.81 ± 1.13	4.43 ± 1.09	2.95 ± 1.34	5.41 ± 1.12	4.77 ± 1.69	6.18 ± 1.21
S53a	31.50 ± 2.03	55.34 ± 3.59	55.84 ± 3.90	51.82 ± 3.58	29.51 ± 2.34	45.68 ± 2.44
S53b	31.50 ± 2.03	4.24 ± 2.52	1.14 ± 2.97	9.07± 2.82	29.51 ± 2.34	12.21 ± 3.82
S84a	69.90 ± 2.24	68.11 ± 2.64	21.78 ± 2.06	-7.34 ± 2.29	-25.03 ± 3.06	-1.15 ± 2.50
S84b	-22.45 ± 2.53	-19.67 ± 2.75	21.78 ± 2.06	54.91± 2.20	71.85 ± 2.51	47.48 ± 2.47
S85a	73.12 ± 2.15	31.13 ± 3.29	34.13 ± 3.68	59.05 ± 5.85	72.54 ± 2.28	101.53 ± 3.80
S85b	73.12 ± 2.15	106.96 ± 3.39	99.75 ± 2.87	87.84± 3.10	72.54 ± 2.28	45.87 ± 3.13
S89a	52.14 ± 8.76	27.99 ± 5.64	-25.75 ± 8.10	-48.08 ± 4.31	-65.28 ± 6.26	59.86 ± 7.67
S89b	-20.04 ± 5.23	10.07 ± 7.17	43.42 ± 5.42	66.46± 4.08	85.63 ± 4.75	-10.17 ± 7.02
S91	75.36 ± 1.44	81.10 ± 2.27	81.19 ± 1.91	83.45 ± 1.61	83.22 ± 1.91	84.46 ± 1.62
S96	-7.70 ± 2.77	-27.13 ± 2.98	7.54 ± 2.12	-52.30 ± 2.54	-76.51 ± 2.62	-13.99 ± 2.95

Table 7. Radial velocities of the candidate binary systems identified in the λ Ori cluster sample.

	JD-2453600.00							
	58.86	59.86	60.84	84.82	86.78	86.82	86.85	97.74
ID	RV (km/s)	RV (km/s)	RV (km/s)	RV(km/s)	RV (km/s)	RV (km/s)	RV (km/s)	RV (km/s)
L01	25.41±1.06	29.09±1.25	24.36±1.05	25.65±0.97	24.05±0.74	25.03±1.16	24.98±0.91	24.31±1.46
L03	19.48±0.41	20.98±0.49	20.13±0.37	20.91±0.41	20.89±0.54	20.91±0.75	21.01±0.62	32.16±0.92
L10a	27.18±0.66	29.27±1.44	28.14±0.73	-1.29±1.88	-2.48±1.90	-1.66±2.06	-1.33±1.90	26.59±0.66
L10b	27.18±0.66	29.27±1.44	28.14±0.73	30.49±2.80	29.34±2.99	29.71±2.57	29.19±2.58	26.59±0.66
L22	24.40±1.43	28.26±2.58	29.54±1.31	24.54±1.67	27.19±1.15	27.57±0.97	27.60±0.88	23.27±1.33
L32	25.41±2.88	24.66±3.28	16.12±3.85	28.19±2.63	25.35±2.98	24.67±3.96	25.16±2.67	34.81±5.05

Table 8. Binary systems parameters for the 6 binaries in the σ Ori cluster for which a sinusoidal fit of the RV curves was performed. Errors are 1σ

ID	$V_\circ^a$ (km/s)	P^b (days)	K_1^c (km/s)	K_2^c (km/s)	$a_1 \sin i^d$ ($R_\odot$)	$a_2 \sin i^d$ ($R_\odot$)	f(M)^e ($M_\odot$)	M_1/M_2^f
S29	32.06 ± 0.73	8.72 ± 0.02	25.4 ± 1.3	41.7 ± 1.3	4.38 ± 0.22	7.18 ± 0.22	0.015 ± 0.002	1.64 ± 0.10
S53	30.61 ± 1.06	8.52 ± 0.01	29.1 ± 2.8	32.1 ± 2.3	4.90 ± 0.46	5.39 ± 0.39	0.022 ± 0.006	1.10 ± 0.13
S84	23.43 ± 0.69	6.07 ± 0.01	43.8 ± 1.3	43.8 ± 1.3	5.25 ± 0.16	5.25 ± 0.16	0.053 ± 0.005	1.00 ± 0.04
S85	72.34 ± 0.88	12.78 ± 0.02	35.3 ± 2.3	43.0 ± 2.3	8.91 ± 0.59	10.84 ± 0.59	0.058 ± 0.012	1.22 ± 0.10
S89	16.54 ± 2.02	13.82 ± 0.04	69.8 ± 4.4	86.5 ± 4.4	19.02 ± 1.19	23.59 ± 1.20	0.486 ± 0.092	1.24 ± 0.10
S96	−34.79 ± 1.19	3.895 ± 0.004	43.4 ± 1.6	...	3.33 ± 0.12	...	0.033 ± 0.004	...

a: velocity of the binary system center of mass
b: period of the binary system
c: semi-amplitude of the RV curve
d: semi-major axis of the binary orbit
e: binary system mass function
f: mass ratio of the binary components

$V_F = 43$ km s^{-1} and $\sigma_F = 37$ km s^{-1}. In the case of λ Ori we obtain $V_C = 27.03$ km s^{-1} with $\sigma_C = 0.49$ km s^{-1} for the cluster and $V_F = 22$ km s^{-1} with $\sigma_F = 9$ km s^{-1} for the field, although, considering the low number of field stars in the λ Ori sample, the parameters of the latter distribution are poorly determined. For each cluster, we classify a star as member if its RV, taking the error bar into account, differs by less than $3\sigma_C$ from the cluster average velocity V_C. Using this criterion, among the 93 stars in the σ Ori sample we find 64 stars with RV consistent with membership, while among the 44 stars in the λ Ori sample, 37 have RV consistent with membership. The membership of the 10 binaries excluded from the RV distributions is undetermined. The expected contamination of the σ Ori member sample by non-members, estimated by integrating the field star distribution between $V_C - 3\sigma_C$ and $V_C + 3\sigma_C$, is ∼2 stars.

The velocity of the σ Ori cluster is in agreement with that of its central high-mass star σ Orionis (27 ± 4 km s^{-1}, Morrell & Levato 1991) and with the cluster mean velocity found by Zapatero Osorio et al. (2002), Kenyon et al. (2005) and Jeffries et al. (2006). Our measurements do not evidence the presence of the kinematically-separated ($V_r = 23.8 \pm 1.1$ km s^{-1}) young stellar population discovered by Jeffries et al. (2006). Since this second population is concentrated to the north-west of the hot star, this apparent disagreement can be attributed to the different positions of the observed fields. In fact, if we limit the analysis to the Jeffries et al. (2006) field with the largest area in

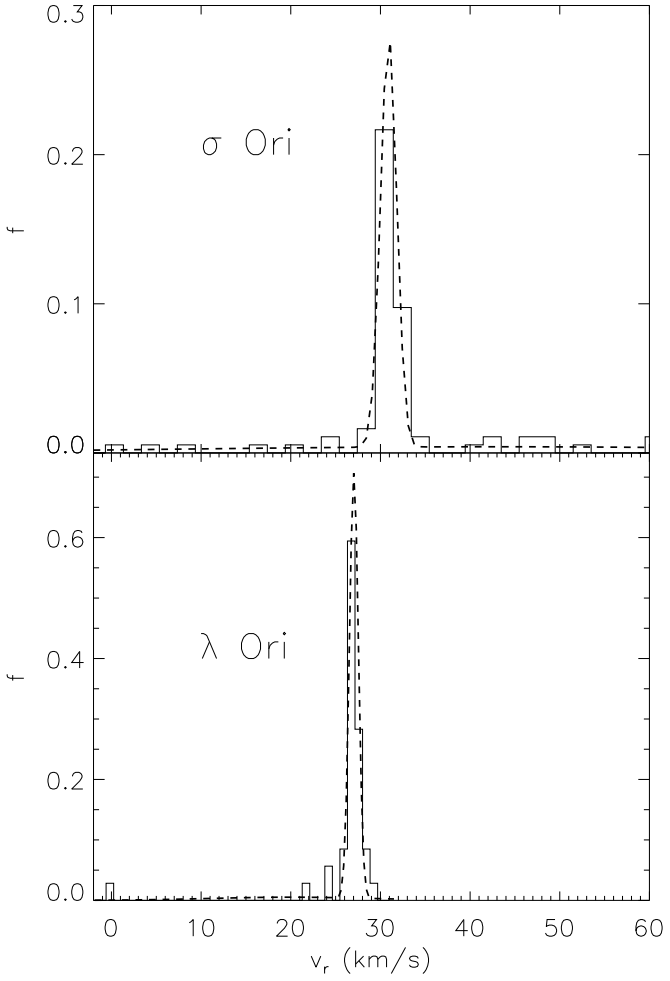

Fig. 5. Radial velocity distribution of the observed sources in the two clusters. Only single stars and the binaries of Table 8 are included. The dashed curves are the functions resulting from the fit of the velocity distribution with a weighted sum of two Gaussians.

common with our field, and compute the number of stars in the two RV ranges (20-27 and 27-35 km/s) defined by Jeffries et al. (2006) for the two populations, we find in our field a ratio (3/65 or 5±3%) consistent with that found by Jeffries et al. (2006) (4/46 or 9±4%). The velocity of the λ Ori cluster is in agreement with that found by Dolan & Mathieu (1999) (24.3 ± 2.8 km s^{-1}), but slightly lower than the velocity of its high-mass central star λ Orionis (30.10 ± 1.30 km s^{-1}, Kharchenko et al. 2007).

Late-type stars ($0.08 - 0.5 M_{\odot}$) deplete their photospheric lithium during the pre-main sequence (PMS) phase (Bodenheimer 1965; Siess et al. 2000), therefore the presence of strong Li absorption at 6708 Å in young clusters can be used as an independent criterion to identify cluster members. Figure 6 shows the Li pEWs measured in the two clusters as a function of the $R-I$ color. Since in all cases where the Li line was not clearly identified the Li pEW turned out to be less than 250 mÅ, we fixed the threshold for selecting cluster members at this value. For the double-lined binaries and for the star L48, for which we cannot measure the Li pEW, we established the membership only by considering whether the Li absorption feature can be identified or not. As shown in Fig. 6, the bulk of the measured pEWs above the chosen threshold is located around a median

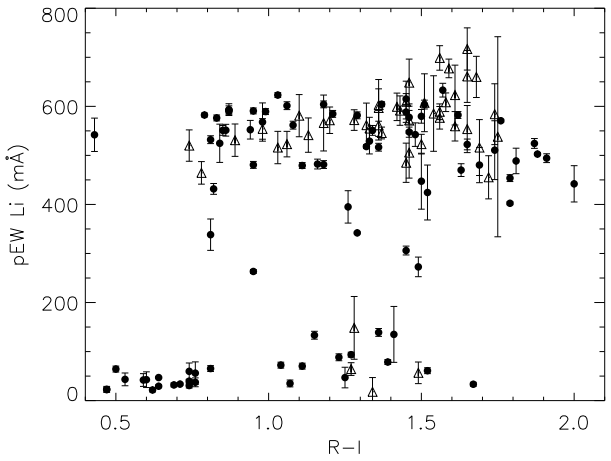

Fig. 6. Li pEWs vs. $R-I$ for the stars of the σ Ori (filled circles) and λ Ori (open triangles) cluster samples with available optical photometry.

value of 560 mÅ with a dispersion of ∼100 mÅ. According to the curves of growth derived by Palla et al. (2007) for a sample of stars observed by GIRAFFE and very similar to that described in this paper, this median pEW is compatible with the full preservation of lithium. In the σ Ori cluster, we found a few sources with pEWs between 250 and 400 mÅ. As shown by Sacco et al. (2007), these low pEWs are mainly due to spectral veiling, but we cannot exclude the presence of some partially-depleted stars. This hypothesis is supported by the discovery of three highly-depleted stars among the σ Ori cluster members, reported by Sacco et al. (2007).

Young K and M stars show emission in Hα due to accretion and chromospheric activity (Barrado y Navascués & Martín 2003). Therefore we used the presence of Hα in emission as the third criterion to identify cluster members. Although, due to the very low S/N, we have not been able to subtract the correct emission of the sky from the spectrum of the star L48 (see Sect. 2.5), this star has been classified as a member, considering that the Hα emission line observed in its spectrum is nearly two times larger than the Hα line observed in the sky spectrum.

In Tables 1 and 2, for the σ Ori and λ Ori clusters respectively, we give the results of our membership selection from the individual criteria mentioned above, together with a final membership assessment derived from the comparison of the three criteria, which in most cases agree. In Table 1 we also indicate if the X-ray counterparts of the stars have been detected by *XMM-Newton*. For the probable binaries with undetermined RV, we relied only on the Li and Hα criteria, considering as possible members those stars for which both Li and Hα indicate membership, although we cannot exclude their belonging to a separate young population present in the same area. In the σ Ori sample, we classify 62 stars as members or possible members and 29 stars as non-members. In λ Ori, we find 42 members or possible members and 2 non-members. For the remaining 7 stars in σ Ori and 5 stars in λ Ori, the three criteria do not agree, and we assigned a final membership based on the following considerations:

– star S37 in σ Ori has a RV inconsistent with membership, but it appears to be a PMS star both for Hα and Li, as well as for the presence of X-ray emission, which supports its youth. Its RV ($V_{\rm r} = 23.73 \pm 0.45$ km s^{-1}) is similar to that of the second population discovered by Jeffries et al. (2006) close to

the σ Ori cluster ($V_r = 23.8 \pm 1.1$ km s^{-1}), therefore this star might belong to this separate population in the Orion OB1 association. On the other hand, Zapatero Osorio et al. (2002) found for S37 a RV of 33 ± 7 km s^{-1}, which is not consistent with the value measured by us, suggesting that this star might be a binary system. Although this second hypothesis cannot be excluded, the excellent agreement of our precise RV measurement with the RV of the second population from Jeffries et al. (2006) and the absence of any sign of binarity in our observations lead us to believe the first hypothesis more likely, therefore we classify this star as a probable non-member.

- in λ Ori, stars L11, L12 and L31 have RV inconsistent with membership, but Hα and Li consistent with them being PMS stars. In the case of L12, Dolan & Mathieu (1999) found a different RV of 30.52 km s^{-1}; considering that no other young stellar population has been discovered in the region of the λ Ori cluster, this star is likely a binary, therefore it has been classified as a possible member. We classified also L11 and L31 as a possible cluster members, considering that their RV differs from the mean velocity of the cluster by less than 5σ.
- the three stars S84, L05 and L13 are not members according to RV and Li, but show Hα in emission. They probably are older chromospherically active field stars, therefore they are classified as non-members.
- stars S22 and S31 have RVs consistent with membership, but show Hα in absorption and no signs of Li absorption, so we have classified these sources as non-members;
- stars S55, S59 and S75 are cluster members according to RV and Hα, but their Li pEWs are below the threshold chosen for the membership selection. As discussed in detail by Sacco et al. (2007), these 3 stars can be classified as cluster members also on the basis of other membership indicators.

In conclusion, in the σ Ori sample we find 65 members or possible members and 33 non-members, while in the λ Ori sample we find 45 members or possible members and 4 non-members. The higher contamination found in the σ Ori sample can be ascribed to the target selection method. Indeed, as shown in the color-magnitude diagram (CMD) plotted in Fig. 7, the σ Ori sample includes a large number of stars located below the 10−20 Myr isochrones, nearly all of which turned out to be non-members. Stars below the 10−20 Myr isochrones are not included in the Barrado y Navascués et al. (2004) and Dolan & Mathieu (1999) catalogues, from which we retrieved the λ Ori targets.

We have compared our results with the previous membership information available in the literature (see Sect. 2.1). In the case of σ Ori, among the 18 members selected on the basis of previous spectroscopic information, we confirm membership for all of them, except for the star S37, which has been classified as a non-member because of its RV (see above). Of the 66 candidates selected only by means of the photometric data, only 47 are confirmed spectroscopically as members, while the remaining 19 resulted to be non-members. For the remaining 14 targets which appear to be non-members on the basis of photometry, we confirm that 13 of them are indeed not members of the cluster. The remaining star (S47) has been classified by us as a member, because it has all spectroscopic indicators consistent with membership, and is also an X-ray source. However its position in the CMD is anomalous, falling below the ZAMS (see Fig. 7). Given the spectroscopic and X-ray evidence, we believe that its photometric data, retrieved from Wolk (1996), might be wrong, therefore its photometry will not be taken into account in the following sections.

For λ Ori, we find that all the targets selected by means of previous spectroscopy from Dolan & Mathieu (1999) (15 stars) and Barrado y Navascués et al. (2004) (3 stars) are confirmed as members, while among the candidates selected only by means of photometry we find 26 members or probable members and 4 non-members.

3.3. Accretion properties

In Tables 4 and 5 we report, for σ Ori and λ Ori respectively, all data concerning accretion, outflow and disk signatures, namely, the Hα width at 10% of the peak, the pEWs of Hα and the pEWs of the HeI emission lines, generally interpreted as due to the accretion flow, the pEWs of the forbidden NII and SII lines at 6583, 6716 and 6731 Å, which are signatures of outflow material and, in the last column, the *Spitzer* classification performed by Hernández et al. (2007) and Barrado y Navascués et al. (2007), using the criterion defined by Lada et al. (2006) based on the slope α of the spectral energy distribution between 3.6 and 8.0 μm, where $\alpha = \mathrm{d}\log(\lambda F_\lambda)/\mathrm{d}\log(\lambda)$[2]. In Tables 4 and 5 we also give the accretion rates derived from Eq. (1) for every star harboring a circumstellar disk with an Hα width at 10% of the peak larger than 200 km s^{-1}. In the σ Ori cluster, MARs range between $10^{-11} M_\odot$ yr^{-1} and $10^{-7.7} M_\odot$ yr^{-1}, while in the λ Ori cluster they range between $10^{-11} M_\odot$ yr^{-1} and $10^{-10.1} M_\odot$ yr^{-1}.

The Hα pEWs as a function of the Hα widths at 10% of the peak are shown in Fig. 8, where stars harboring a circumstellar disk are indicated by filled symbols. As can be seen in this figure and in Tables 4 and 5, we find some stars with an Hα larger than 200 km s^{-1} without any other accretion signature and classified as class III objects by the *Spitzer* data. This result is likely due to the presence of absorption bands in the Hα spectral region, which causes an overestimate of the Hα width, and to the rotational broadening (the stars L16 and L33, which are the most relevant cases have v sin $i \sim 60$ km/s). We also find some stars with Hα larger than 200 km s^{-1} but with a low pEW (S23 and S47 is the most relevant case), and stars in the opposite situation (S93 and S94 are the most relevant cases). The former result is mainly due to the presence of intense absorption features overlapping the emission ones as already pointed out by Sicilia-Aguilar et al. (2006) for some CTTSs belonging to the Tr37 cluster, while the latter result is due to the presence of accretion flows only in the direction perpendicular to the line of sight.

We also observed the λ Ori sources in the spectral range including the CaII infrared triplet, which can also be used to measure MARs (Mohanty et al. 2005), but in the whole sample we do not find any star clearly showing CaII emission due to accretion.

4. Discussion

4.1. Disk properties in σ Ori and λ Ori

As mentioned in Sect. 2.1 in the σ Ori sample there are 78 sources in common with the Hernández et al. (2007) catalogue of cluster members and 5 sources in common with the catalogue of uncertain members. According to our membership analysis, in

[2] Stars with $\alpha > 0$ are classified as protostars (class I), those with $-1.8 < \alpha < 0$ as objects with a thick disk (class II), those with $-2.56 < \alpha < -1.8$ as objects with a thin and evolved circumstellar disk (EV) and those with $\alpha < -2.56$ are classified as diskless objects (class III)

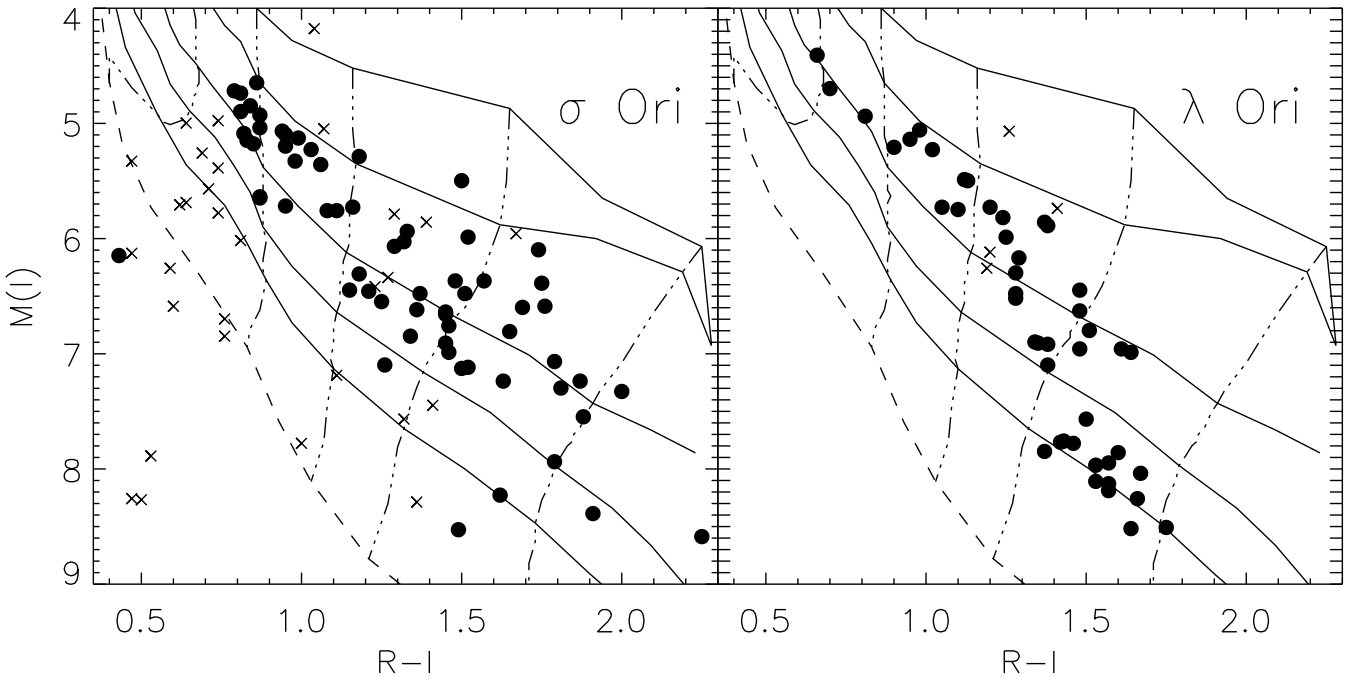

Fig. 7. CMD of the observed targets in the σ Ori (left panel) and λ Ori (right panel) cluster. Filled circles and crosses indicate, respectively, members and non-members of the two clusters. Stellar magnitudes are corrected for the distance and reddening as in Fig. 1. Continuous, dashed and dot-dashed lines represent the isochrones at 1, 2, 5, 10 and 20 Myr, the Zero Age Main Sequence (ZAMS) and evolutionary tracks at 0.2, 0.3, 0.4, 0.6, 1.0 $M_{\odot}$ from the Siess et al. (2000) models, respectively.

the former catalogue there are 62 members and 16 non-members, while in the latter one there are 3 members and 2 non-members. Given that 20% of the stars in common with our catalogue are non-members, the number of σ Ori members included in the Hernández et al. (2007) catalogue, selected using mainly photometric data, is likely overestimated, and, therefore, the fraction of T Tauri stars ($0.1 - 1.0 M_{\odot}$) with disks (36±4%) derived by them is likely underestimated. In the λ Ori cluster, we have 44 sources in common with the Barrado y Navascués et al. (2007) catalogue, 40 classified as members and 4 as non-members according to our analysis.

According to the disk classification by Hernández et al. (2007) and Barrado y Navascués et al. (2007), among the σ Ori cluster members we have 1 protostar, 28 stars with thick disks, 5 stars with evolved disks and 31 diskless stars, while in λ Ori we have 7 stars with thick disks, 4 with evolved disks and 29 diskless stars. Therefore, in the mass range 0.2-1.0 $M_{\odot}$, the fraction of stars with disks in the σ Ori cluster (52±9%) is larger than in the λ Ori one (28±8%).

The discrepancy between the two clusters does not depend on the analysis method, because we compare the two clusters using homogeneous data and the same selection criteria both for membership and disk classification. We can also exclude that this result might be due to a bias in the target selection against the diskless stars. In fact, for both clusters the observed stars have been retrieved from catalogues of candidate members selected through CMDs and spectroscopic membership indicators (lithium and RVs), which do not depend on disk and accretion properties.

Another possible bias in the target selection can be present against the older stars, which are more likely class III objects. However, in contrast with our results, this kind of bias should affect more strongly the λ Ori sample than the σ Ori one. In fact, as pointed out in Sect. 2.1 and 3.2, the λ Ori targets are selected mainly from the Barrado y Navascués et al. (2004) catalogue which includes only stars around the 5 Myr isochrone (Baraffe et al. 1998 models at 400 pc), while the σ Ori target sample includes stars in a larger age range (0−20 Myr). Moreover, the agreement between the fraction of stars with disks in our sample (28±8%) and in the sample of all stars in the magnitude range 11.3< J <14.8 (105 stars) included in the Barrado y Navascués et al. (2007) catalogue (22±5%) confirms that our sample is not affected by target selection biases. On the other hand, the disagreement between the fraction of stars with disks found in the σ Ori sample (52±9%) and that obtained, in a very similar magnitude range (11.5< J <14.6) by Hernández et al. (2007) (36.3±4.1%), confirms that, as we argued above, their sample of cluster members is contaminated by a large number of field stars.

The fraction of stars with disks found by us in σ Ori is in agreement with that found by Caballero et al. (2007) for the brown dwarfs (47±15%). This suggests that the disk frequency does not depend on mass over the interval 0.02−1.0 $M_{\odot}$.

4.2. Accretion properties in σ Ori and λ Ori

In Table 9 we compare the disk and accretion properties of σ Ori and λ Ori on the basis of all the different disk and accretion classifications. Furthermore, in the last two columns, we compare the fraction of active disks, namely, the fraction of accreting objects among the stars harboring a circumstellar disk (class I, class II and EV).

The data reported in Table 9, together with the comparison between the accretion rates measured by means of the Hα widths at 10% of the peak, prove that, in spite of the similarities between the two clusters, the disk and accretion properties of their low-mass stellar populations are very different. Specifically, in the σ Ori cluster we find a larger fraction of stars with disks, a larger

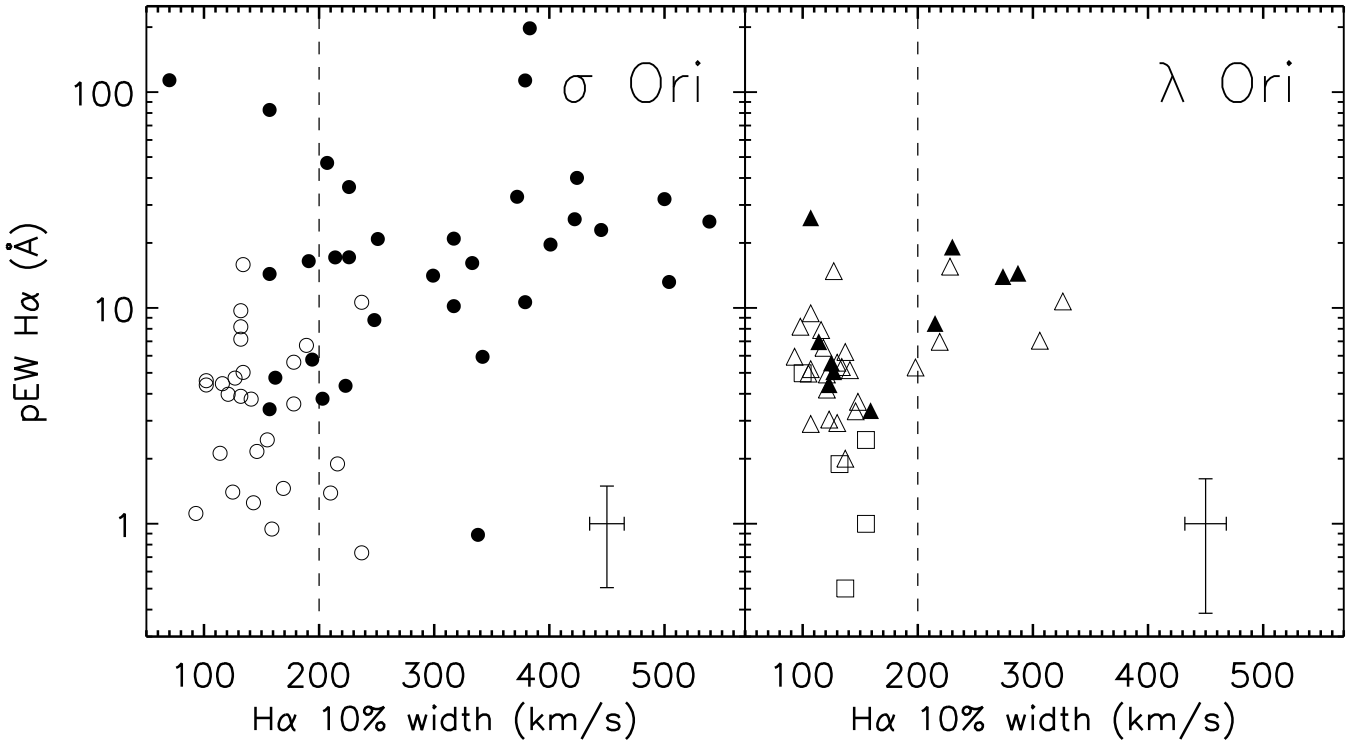

Fig. 8. Hα pEW as a function of the Hα width at 10% of the peak measured from the summed spectra of the σ Ori (left panel) and λ Ori (right panel) cluster members. Filled and open symbols represent stars with and without a circumstellar disk according to the *Spitzer* data, while squares in the left panel represent stars without *Spitzer* photometry. Median error bars are reported on the bottom-right corner.

Table 9. Disk and accretion properties[a] in σ Ori and λ Ori

	Disk	Thick Disk	Hα width[b]	HeI 6678 Å	other lines	active disk (Hα)[c]	active disk (He I)
σ Ori	52± 9%	45± 8%	42±8%	35±7%	37±8%	78±16%	65±14%
	(34/65)	(29/65)	(25/60)	(22/63)	(23/63)	(25/32)	(22/34)
λ Ori	28± 8%	18± 7%	10±5%	7±4%	12±5%	40±20%	27±16%
	(11/40)	(7/40)	(4/39)	(3/43)	(5/43)	(4/10)	(3/11)

a: Errors are calculated as $\sqrt{N}$/total.
b: H$\alpha_{10\%}$ >200 km/s
c: Stars harbouring a circumstellar disk with H$\alpha_{10\%}$ >200 km/s
c: Stars harbouring a circumstellar disk with He I in emission

fraction of accreting objects, and larger accretion rates than in λ Ori. Furthermore, the last two columns of Table 9 show that the two clusters differ also if we consider only the subsample of stars with a circumstellar disk.

4.3. The effects of the high-mass stars and of the supernova explosion in the λ Ori cluster.

Dolan & Mathieu (1999, 2001) already evidenced the lack of strong Hα emitters in the λ Ori cluster and the existence of a discrepancy with the fraction of CTTSs observed in the B30 and B35 clouds, located 2.2° and 2.7° from the central star λ Orionis. They supposed that, as observed in the Trapezium around θ^1 Ori (Johnstone et al. 1998), circumstellar disks could have been photo-evaporated by the far-UV radiation of the high-mass stars in the period before the supernova explosion, when high and low-mass stars were confined by the parent cloud in a smaller region. The same effect might have not affected the σ Ori stars because its central high-mass star is less bright than λ Orionis, and likely also than the supernova progenitor and because the σ Ori cluster might never have been confined in a smaller region as Dolan & Mathieu (1999, 2001) supposed for the λ Ori cluster.

However, recent N-body simulations showed that the effect of photoevaporation of the circumstellar disks due to emission from the high-mass stars is negligible for clusters composed of less than 1000 members (Adams et al. 2006), while Barrado y Navascués et al. (2004) found only 170 candidate members in their survey over an area of 0.3 deg^2 (with a completeness limit of 0.025 $M_\odot$), including most part of the λ Ori cluster. Moreover, Barrado y Navascués et al. (2007) found several stars with disks near the central O stars and no correlation between the fraction of stars with disks and the distance from λ Orionis.

Furthermore the difference in the accretion properties of stars with disks in the two clusters, discussed in Sect. 4.2, does not support the Dolan & Mathieu (2001) hypothesis, because the far-UV radiation of high-mass stars could trigger the disk pho-

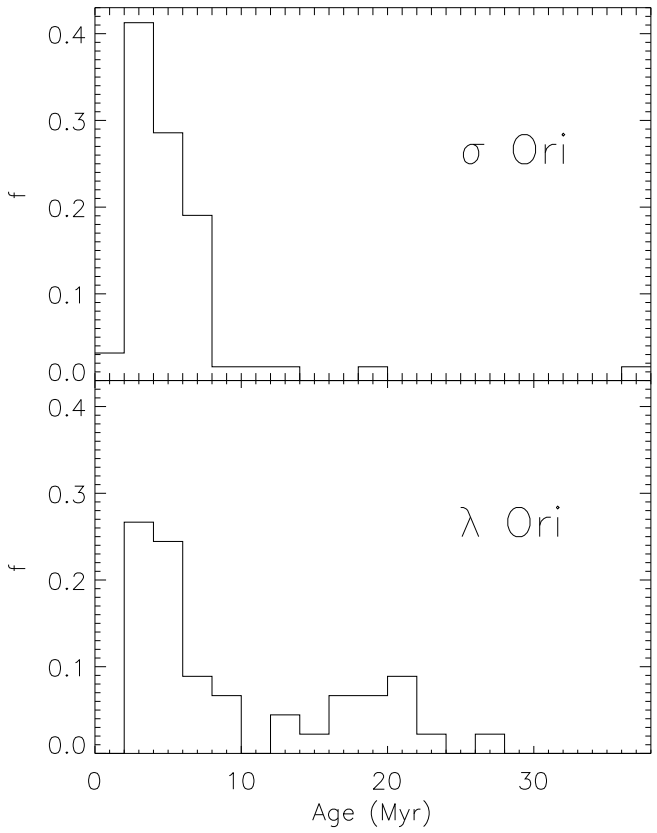

Fig. 9. Age distribution of the members selected in σ Ori and λ Ori. Ages were derived from the R and I magnitudes using Siess et al. (2000) evolutionary models. As discussed in the text, the age distributions shown in this figure are not in agreement with the Li line pEWs shown in Fig. 6.

toevaporation but should not directly influence the accretion on the stars. On the contrary, Fatuzzo et al. (2006) suggested that a supernova explosion could increase the MARs of the nearby stars. Specifically, they hypothesized that the enhancement of the cosmic rays flux following a supernova explosion causes in the circumstellar disks of the nearby stars an increase of the ionization levels and, therefore, of the magneto-rotational instabilities, which, according to the Gammie (1996) model, trigger the accretion on the CTTSs

4.4. The age hypothesis

Another possibility is that the discrepancy between the two clusters could be due to a different age. As shown by Hernández et al. (2007) using *Spitzer* photometry and by Haisch et al. (2001) using J, H, K and L bands photometry, the fraction of stars with disks decreases from 100% in the youngest regions to a few percent in 6−7 Myr old clusters. Moreover, Hernández et al. (2007) and Barrado y Navascués et al. (2007) found a larger fraction of evolved thin disks in the older young clusters. Since a significant fraction of these evolved disks might have stopped the accretion onto the stars (Sicilia-Aguilar et al. 2006 and references therein), it is likely that in young clusters the fraction of non-accreting disks grows with age. Following these considerations, the suggestion that the λ Ori population is more evolved than the σ Ori one could well explain the differences between the two clusters.

To investigate this hypothesis, we plot in Fig. 9 the age distributions of the members selected in both clusters. Ages have been calculated from the Siess et al. (2000) evolutionary models using the I and R magnitudes, while for the distance modulus and the reddening we used the same values as in Fig. 1. The two histograms clearly show that the λ Ori population is older than the σ Ori one. Moreover, the CMD for the two clusters, shown in Fig. 7, evidences that the age difference concerns especially the lowest mass stars.

Although Fig. 9 seems to confirm the age hypothesis, we note that the age distributions shown in Fig. 9 could be affected by large sources of errors: the reddening due to the presence of the circumstellar disks could cause an underestimate of the age, while veiling due to accretion could cause an overestimate of age; errors on distances, which are poorly determined in both clusters, could strongly affect the age distributions and, as shown by Hillenbrand et al. (2008), different evolutionary models give different results. The presence of some CTTSs among the oldest and lowest stars in λ Ori confirms that ages derived from R and I magnitudes are affected by these sources of errors, in fact errors due to accretion veiling strongly affects the low-mass stars (Herczeg & Hillenbrand 2008). Moreover, taking into account that, according to the Siess et al. (2000) models, stars in the mass range 0.3−0.2 $M_{\odot}$ deplete very rapidly their photospheric lithium after 15−30 Myr, the oldest stars of the λ Ori cluster in this mass range should have depleted part of their lithium, but, as shown in Fig. 6, the lithium pEWs of λ Ori members are never below 450 mÅ.

More detailed HR diagrams based on spectral types derived from low-resolution spectroscopy are required to better investigate the age difference between the two clusters.

5. Summary and conclusions

In this paper we have reported the results of FLAMES/VLT optical spectroscopic observations of 147 low-mass stars, in the 0.2−1.0 $M_{\odot}$ mass range, belonging to the two very similar clusters σ Ori and λ Ori.

Using RVs, Hα and Li line pEWs, we identified 65 bonafide members of the σ Ori cluster and 45 members of λ Ori. Furthermore we discovered 16 new binary systems and binary candidates, 10 of which are probable members of the clusters and measured rotational velocities of 20 stars. To study the accretion properties, we estimated the stellar MARs from the width at 10% of the peak of the Hα line and measured the pEWs of the Hα and other emission lines, which are signatures of accretion/outflow phenomena. We compared our results with the *Spitzer* observations of the two clusters by Hernández et al. (2007) and Barrado y Navascués et al. (2007), finding that: a) the fraction of stars with disks obtained by Hernández et al. (2007) is likely underestimated due to the presence of a large number of field stars in their catalogue of members; b) the fraction of stars with a circumstellar disk in the σ Ori cluster (52±9%) is larger than in λ Ori (28±8%); c) the fraction of active disks in σ Ori (78±16%) is larger than in λ Ori (40±20%). We have discussed two hypotheses that could explain the discrepancy between the two clusters: either the circumstellar disks in the λ Ori cluster dissipate more rapidly due to the effect of the massive stars emission or the λ Ori cluster could be older and more evolved than σ Ori. The former hypothesis is in contradiction with some theoretical and observational studies, while the latter one cannot be confirmed due to the uncertainties in stellar ages. Further low-resolution spectroscopic observations are required to reach a firm conclusion.

Acknowledgements. We thank the anonymous referee and Antonella Natta for useful suggestions and comments. We acknowledge the staff of the ESO Data Management and Operations department, who performed our observations in service mode.

This work makes use of results produced by the PI2S2 Project managed by the Consorzio COMETA, a project co-funded by the Italian Ministry of University and Research (MIUR) within the Piano Operativo Nazionale "Ricerca Scientifica, Sviluppo Tecnologico, Alta Formazione" (PON 2000-2006). More information is available at http://www.pi2s2.it and http://www.consorzio-cometa.it.

This research has been supported by an INAF grant on *Stellar clusters as probes of star formation and early stellar evolution (PI: F. Palla).* This publication makes use of data products from the Two Micron All Sky Survey, which is a joint project of the University of Massachusetts and the Infrared Processing and Analysis Center/California Institute of Technology, funded by the National Aeronautics and Space Administration and the National Science Foundation.

References

Adams, F. C., Proszkow, E. M., Fatuzzo, M., & Myers, P. C. 2006, ApJ, 641, 504
Baraffe, I., Chabrier, G., Allard, F., & Hauschildt, P. H. 1998, A&A, 337, 403
Barrado y Navascués, D., Béjar, V. J. S., Mundt, R., et al. 2003, A&A, 404, 171
Barrado y Navascués, D. & Martín, E. L. 2003, AJ, 126, 2997
Barrado y Navascués, D., Stauffer, J. R., Bouvier, J., Jayawardhana, R., & Cuillandre, J. C. 2004, ApJ, 610, 1064
Barrado y Navascués, D., Stauffer, J. R., Morales-Calderón, M., et al. 2007, ApJ, 664, 481
Béjar, V. J. S., Martín, E. L., Zapatero Osorio, M. R., et al. 2001, ApJ, 556, 830
Béjar, V. J. S., Zapatero Osorio, M. R., & Rebolo, R. 2004, AN, 325, 705
Blecha, A. & Simond, G. 2004, Giraffe BLDRS Software: Reference Manual (ver. 1.12; Genève: Obs. Genève)
Bodenheimer, P. 1965, ApJ, 142, 451
Burningham, B., Naylor, T., Littlefair, S. P., & Jeffries, R. D. 2005, MNRAS, 356, 1583
Caballero, J. A. 2007, A&A, 466, 917
Caballero, J. A., Béjar, V. J. S., Rebolo, R., et al. 2007, A&A, 470, 903
Diplas, A. & Savage, B. D. 1994, ApJS, 93, 211
Dolan, C. J. & Mathieu, R. D. 1999, AJ, 118, 2409
Dolan, C. J. & Mathieu, R. D. 2001, AJ, 121, 2124
Dolan, C. J. & Mathieu, R. D. 2002, AJ, 123, 387
Duerr, R., Imhoff, C. L., & Lada, C. J. 1982, ApJ, 261, 135
Fatuzzo, M., Adams, F. C., & Melia, F. 2006, ApJ, 653, L49
Franciosini, E., Pallavicini, R., & Sanz-Forcada, J. 2006, A&A, 446, 501
Gammie, C. F. 1996, ApJ, 457, 355
Gomez, M. & Lada, C. J. 1998, AJ, 115, 1524
Gray, D. F. 1992, The Observation and Analysis of Stellar Photospheres (Cambridge University Press)
Haisch, K. E., Lada, E. A., & Lada, C. J. 2001, ApJ, 553, L153
Hartmann, L., Calvet, N., Gullbring, E., & D'Alessio, P. 1998, ApJ, 495, 385
Herczeg, G. J. & Hillenbrand, L. A. 2008, ApJ,in press
Hernández, J., Hartmann, L., Megeath, T., et al. 2007, ApJ, 662, 1067
Hillenbrand, L. A., Bauermeister, A., & White, R. J. 2008, in ASP Conference Series, Vol. 384, Cool Stars, Stellar Systems and the Sun XIV, ed. G. van Belle, 200
Jeffries, R. D., Maxted, P. F. L., Oliveira, J. M., & Naylor, T. 2006, MNRAS, 371, L6
Johnstone, D., Hollenbach, D., & Bally, J. 1998, ApJ, 499, 758
Kenyon, M. J., Jeffries, R. D., Naylor, T., Oliveira, J. M., & Maxted, P. F. L. 2005, MNRAS, 356, 89
Kenyon, S. J. & Hartmann, L. 1995, ApJS, 101, 117
Kharchenko, N. V., Scholz, R.-D., Piskunov, A. E., Röser, S., & Schilbach, E. 2007, AN, 328, 889
Lada, C. J., Muench, A. A., Luhman, K. L., et al. 2006, AJ, 131, 1574
Mohanty, S., Jayawardhana, R., & Basri, G. 2005, ApJ, 626, 498
Morrell, N. & Levato, H. 1991, ApJS, 75, 965
Munari, U. & Carraro, G. 1996, A&A, 314, 108
Murdin, P. & Penston, M. V. 1977, MNRAS, 181, 657
Natta, A., Testi, L., Muzerolle, J., et al. 2004, A&A, 424, 603
Oliveira, J. M., Jeffries, R. D., & van Loon, J. T. 2004, MNRAS, 347, 1327
Oliveira, J. M., Jeffries, R. D., van Loon, J. T., & Rushton, M. T. 2006, MNRAS, 369, 272
Palla, F., Randich, S., Pavlenko, Y. V., Flaccomio, E., & Pallavicini, R. 2007, ApJ, 659, L41
Pasquini, L., Avila, G., Blecha, A., et al. 2002, The Messenger, 110, 1
Perryman, M. A. C., Lindegren, L., Kovalevsky, J., et al. 1997, A&A, 323, L49
Sacco, G. G., Randich, S., Franciosini, E., Pallavicini, R., & Palla, F. 2007, A&A, 462, L23
Sanz-Forcada, J., Franciosini, E., & Pallavicini, R. 2004, A&A, 421, 715
Scholz, A. & Eislöffel, J. 2004, A&A, 419, 249
Sherry, W. H., Walter, F. M., & Wolk, S. J. 2004, AJ, 128, 2316
Sicilia-Aguilar, A., Hartmann, L., Calvet, N., et al. 2006, ApJ, 638, 897
Sicilia-Aguilar, A., Hartmann, L. W., Hernández, J., Briceño, C., & Calvet, N. 2005, AJ, 130, 188
Siess, L., Dufour, E., & Forestini, M. 2000, A&A, 358, 593
Skrutskie, M. F., Cutri, R. M., Stiening, R., et al. 2006, AJ, 131, 1163
Tonry, J. & Davis, M. 1979, AJ, 84, 1511
Walter, F. M., Wolk, S. J., Freyberg, M., & Schmitt, J. H. M. M. 1997, Memorie della Società Astronomica Italiana, 68, 1081
White, R. J. & Basri, G. 2003, ApJ, 582, 1109
Wolk, S. J. 1996, Ph.D. Thesis
Zapatero Osorio, M. R., Béjar, V. J. S., Martín, E. L., et al. 2000, Science, 290, 103
Zapatero Osorio, M. R., Béjar, V. J. S., Pavlenko, Y., et al. 2002, A&A, 384, 937
Zhang, C. Y., Laureijs, R. J., Chlewicki, G., Wesselius, P. R., & Clark, F. O. 1989, A&A, 218, 231

Table 1. Photometry and membership for the observed sample stars in the σ Ori cluster.

ID	Name[a]	RA[b] (J2000)	DEC[b] (J2000)	I[c]	$R-I$[c]	ref[c]	J[b]	$H-K_s$[b]	SpT[d]	v_r (km/s)	$vsin(i)$ (km/s)	Li pEW[e] (mÅ)	Membership v_r	Li	Hα	Tot	X[f]	Notes
S01	p053834-0239	5 38 34.79	−2 39 30.0	11.91	1.04	2	10.44	0.25	M1.0	46.21±0.64		72±6	N	N	N	N	N	
S02	r053838-0236	5 38 38.22	−2 36 38.4	12.38	0.86	2	11.16	0.15	K8.0*	30.93±0.33	<17.8	551±12	Y	Y	Y	Y	Y	
S03	r053835-0231	5 38 35.47	−2 31 51.7	12.45	0.79	2	11.30	0.17	K7.5	30.60±0.29	<17.0	582±4	Y	Y	Y	Y	Y	
S04	4771-1097	5 38 35.87	−2 30 43.3	12.47	0.81	2	11.24	0.17	K8.0*	?		338±32	?	Y	Y	Y?	Y	SB
S05	4771-0910	5 39 18.83	−2 30 53.1	12.58	0.84	2	11.40	0.30	K9.0	29.14±0.65	$42.7^{+1.6}_{-3.1}$	524±39	Y	Y	Y	Y	Y	
S06	4771-1092	5 39 07.61	−2 32 39.2	12.63	0.81	2	11.30	0.31	K8.0	30.27±0.32	<17.0	532±8	Y	Y	Y	Y	Y	
S07	4771-1075	5 39 05.41	−2 32 30.3	12.66	0.87	2	11.55	0.19	K7.0*	30.40±0.20	<17.4	593±12	Y	Y	Y	Y	Y	
S08	4771-0579	5 39 30.43	−2 35 07.3	12.71	0.74	2	11.61	0.15	K6.5	80.50±0.80		30±5	N	N	N	N	N	
S09	p053933-0236	5 39 33.44	−2 36 41.9	12.73	0.64	2	11.85	0.14	K5.0	−14.01±1.15		29±3	N	N	N	N	N	
S10	r053841-0237	5 38 41.29	−2 37 22.6	12.77	0.87	2	11.46	0.21	K9.5	30.89±0.30	<17.0	592±9	Y	Y	Y	Y	Y	
S11	SWW166	5 38 53.07	−2 38 53.6	12.78	1.07	1	11.62	0.21	M1.0	−0.10±0.52		35±7	N	N	N	N	Y	
S12	r053840-0230	5 38 40.27	−2 30 18.5	12.80	0.94	2	11.51	0.37	M0.0*	31.51±0.36	<17.0	552±19	Y	Y	Y	Y	Y	
S13	4771-0041	5 38 27.26	−2 45 09.7	12.82	0.82	2	11.95	0.85	K7.0*	30.00±0.49	<17.0	431±11	Y	Y	Y	Y	Y	
S14	SWW135	5 39 25.20	−2 38 22.0	12.83	0.95	1	11.31	0.45	M0.5	30.10±0.46	<17.0	480±7	Y	Y	Y	Y	Y	
S15	SWW78	5 38 47.46	−2 35 25.2	12.86	0.99	1	-	0.25	M1.0	30.32±0.40	<17.0	589±6	Y	Y	Y	Y	Y	
S16	r053832-0235b	5 38 32.84	−2 35 39.2	12.88	0.83	2	11.54	0.17	K8.5	30.12±0.27	<17.0	576±6	Y	Y	Y	Y	Y	
S17	4771-0080	5 38 52.01	−2 46 43.7	12.91	0.85	3	11.52	0.35	K9.0	30.51±0.36	<17.0	551±10	Y	Y	Y	Y	Y	
S18	4771-1038	5 39 11.63	−2 36 02.9	12.93	0.95	1	11.62	0.22	K8.0*	30.13±0.28	<17.0	590±6	Y	Y	Y	Y	Y	
S19	r053849-0238	5 38 49.17	−2 38 22.2	12.96	1.03	1	11.39	0.15	M0.5*	30.79±0.28	<17.0	623±5	Y	Y	Y	Y	Y	
S20	4771-0961	5 38 02.21	−2 29 55.6	12.99	0.69	2	11.83	0.19	K6.0	21.24±0.69		32±4	N	N	N	N	N	
S21	SWW102	5 38 47.92	−2 37 19.2	13.02	1.18	1	-	-	M1.0	31.77±0.51	<17.0	481±8	Y	Y	Y	Y	Y	
S22	r053830-0241	5 38 30.60	−2 41 18.8	13.06	0.47	2	12.42	0.12	K2.0	29.17±0.83		22±5	Y	N	N	N	N	
S23	SWW48	5 38 42.28	−2 37 14.8	13.06	0.98	1	11.77	0.22	M0.5	30.42±0.43	<17.0	568±39	Y	Y	Y	Y	N	
S24	SWW36	5 38 43.55	−2 33 25.4	13.09	1.06	1	11.72	0.24	M1.0	31.63±0.33	<17.0	620±23	Y	Y	Y	Y	Y	
S25	4771-1090	5 38 46.05	−2 43 47.8	13.12	0.74	2	11.97	0.16	K6.5	8.38±0.60		39±4	N	N	N	N	N	
S26	SWW205	5 38 49.22	−2 41 25.1	13.23	1.50	1	11.67	0.27	M3.5	?		442±57	?	Y	Y	Y?	Y	SB
S27	r053838-0226	5 38 38.56	−2 26 44.8	13.30	0.71	3	12.30	0.16	K6.0	91.40±0.68		33±2	N	N	N	N	N	
S28	SWW35	5 38 48.68	−2 36 16.2	13.37	0.87	1	12.11	0.20	K9.5	32.53±0.46	<17.0	590±4	Y	Y	Y	Y	Y	
S29	r053851-0236	5 38 51.45	−2 36 20.6	13.38	0.87	2	12.44	0.26	K9.5	32.06±0.73		Y	Y	Y	Y	Y	Y	SB2
S30	K3.01-170	5 38 15.90	−2 34 41.2	13.42	0.64	3	12.37	0.15	K5.0	−30.56±0.70		47±2	N	N	N	N	N	
S31	r053812-0232	5 38 12.60	−2 33 01.5	13.44	0.62	3	12.46	0.16	K5.0	33.15±0.71		21±4	Y	N	N	N	N	
S32	SWW195	5 39 11.52	−2 31 06.6	13.45	0.95	1	11.99	0.46	M0.5	30.91±0.79	<17.0	263±4	Y	Y	Y	Y	Y	
S33	SWW97	5 38 45.38	−2 41 59.4	13.46	1.16	1	11.99	0.29	M1.0	31.86±0.57	<17.0	482±10	Y	Y	Y	Y	Y	
S34	r053831-0235	5 38 31.58	−2 35 14.9	13.49	1.11	1	11.52	0.35	M0.0*	32.13±0.55	<19.2	479±6	Y	Y	Y	Y	Y	
S35	SWW47	5 38 53.17	−2 43 52.8	13.49	1.08	1	12.23	0.20	M1.0	30.48±0.49	<17.0	561±8	Y	Y	Y	Y	Y	
S36	K4.03-511	5 38 19.15	−2 35 27.9	13.51	0.74	3	12.31	0.18	K6.5	121.73±0.67		59±17	N	N	N	N	N	
S37	J053920.5-022737	5 39 20.44	−2 27 36.8	13.52	1.29	1	12.15	0.26	M2.0*	23.73±0.45		581±7	N	Y	Y	N?	Y	
S38	SWW71	5 38 55.44	−2 41 29.7	13.59	1.39	1	12.17	0.28	M3.0	3.53±0.54		78±5	N	N	N	N	N	
S39	SWW87	5 38 27.74	−2 43 01.0	13.67	1.33	1	12.19	0.16	M2.5	29.91±0.58	$21.9^{+0.5}_{-3.1}$	549±32	Y	Y	Y	Y	Y	
S40	p053902-0238	5 39 02.16	−2 38 38.2	13.69	1.67	2	12.40	0.16	M4.0	61.34±0.71		33±4	N	N	N	N	N	
S41	r053833-0236	5 38 34.06	−2 36 37.5	13.72	1.52	1	11.98	0.25	M3.5*	34.12±2.21	$45.7^{+1.1}_{-5.3}$	424±56	Y	Y	Y	Y	Y	
S42	p053925-0231	5 39 25.34	−2 31 43.7	13.75	0.81	2	12.43	0.26	K8.0	103.44±0.61		65±6	N	N	N	N	N	
S43	SWW41	5 38 08.27	−2 35 56.3	13.76	1.32	1	12.14	0.33	M2.5	?		518±4	?	Y	Y	Y?	Y	SB
S44	SWW50	5 38 31.41	−2 36 33.8	13.80	1.29	1	12.17	0.49	M2.0	30.81±0.88	<17.0	342±2	Y	Y	Y	Y	N	
S45	K1.02-7	5 38 48.29	−2 36 41.0	13.83	1.74	3	12.04	0.26	M4.5	30.21±1.38	$32.1^{+12.4}_{-7.1}$	510±60	Y	Y	Y	Y	Y	
S46	r053832-0235a	5 38 32.60	−2 35 04.1	13.86	0.47	3	13.27	0.17	K2.0	51.92±1.49		23±6	N	N	N	N	N	
S47	r053834-0234	5 38 34.31	−2 35 00.1	13.88	0.43	2	-	-	K1.0	30.37±0.38	$29.3^{+2.8}_{-5.6}$	542±34	Y	Y	Y	Y	Y	

Table 1. continued

ID	Name[a]	RA[b] (J2000)	DEC[b] (J2000)	I[c]	$R-I$[c]	ref[c]	J[b]	$H-K_s$[b]	SpT[d]	v_r (km/s)	$vsin(i)$ (km/s)	Li pEW[e] (mÅ)	Membership v_r	Li	Hα	Tot	X[f]	Notes
S48	r053814-0235	5 38 14.23	−2 35 07.3	13.99	0.59	3	13.11	0.11	K4.5	48.50±0.71		42±13	N	N	N	N	N	
S49	SWW177	5 38 29.12	−2 36 02.7	14.04	1.18	1	-	-	M1.0	32.46±0.43	<17.0	604±7	Y	Y	Y	Y	Y	
S50	SWW88	5 38 05.67	−2 40 19.4	14.07	1.27	1	12.77	0.28	M2.0	?		94±5	?	N	N	N	N	SB
S51	SE34	5 38 50.39	−2 26 47.7	14.10	1.48	1	12.50	0.29	M3.5	30.48±0.57	$21.5^{+6.3}_{-4.5}$	582±23	Y	Y	Y	Y	Y	
S52	SE3	5 38 13.20	−2 26 08.8	14.10	1.57	1	12.48	0.27	M4.0	32.07±0.52	<17.0	633±14	Y	Y	Y	Y	Y	
S53	SWW144	5 38 43.34	−2 32 00.8	14.12	1.75	1	12.24	0.28	M4.5	30.61±1.06		Y	Y	Y	Y	Y	Y	SB2
S54	SWW101	5 38 49.64	−2 45 26.9	14.15	1.23	1	13.15	0.19	M1.5	41.57±0.57		88±7	N	N	N	N	-	
S55	SE51	5 39 17.17	−2 25 43.4	14.18	1.15	1	12.90	0.19	M1.0	29.47±0.48	<17.0	133±8	Y	N	Y	Y	Y	
S56	r053923-0233	5 39 22.87	−2 33 33.1	14.19	1.21	1	12.83	0.26	M2.0*	30.26±0.37	<17.0	584±7	Y	Y	Y	Y	Y	
S57	SWW200	5 38 49.93	−2 41 22.8	14.21	1.37	1	12.75	0.22	M3.0	31.35±0.49	<17.0	604±5	Y	Y	Y	Y	Y	
S58	SWW28	5 39 02.77	−2 29 55.8	14.21	1.51	1	12.61	0.31	M3.5	31.77±0.49	<17.0	603±9	Y	Y	Y	Y	Y	
S59	SWW127	5 39 24.36	−2 34 01.4	14.28	1.25	1	12.98	0.21	M2.0	33.18±0.45	<17.0	47±21	Y	N	Y	Y	Y	
S60	J053836.7-024414	5 38 36.69	−2 44 13.7	14.32	1.76	1	12.54	0.27	M4.5	30.57±0.75	<17.0	570±3	Y	Y	Y	Y	N	
S61	4771-1099	5 39 07.81	−2 40 09.1	14.32	0.60	2	13.57	0.10	K4.5	45.54±1.07		42±16	N	N	N	N	N	
S62	J053820.1-023802	5 38 20.22	−2 38 01.6	14.33	1.69	1	12.58	0.25	M4.0*	33.92±2.54	$56.2^{+7.0}_{-9.8}$	480±36	Y	Y	Y	Y	Y	
S63	J053827.5-023504	5 38 27.51	−2 35 04.2	14.35	1.36	3	12.83	0.25	M3.5*	29.72±0.63	<17.0	516±8	Y	Y	Y	Y	Y	
S64	r053907-0228	5 39 07.59	−2 28 23.4	14.37	1.45	1	12.88	0.19	M3.0*	31.48±0.46	<17.0	615±11	Y	Y	Y	Y	Y	
S65	SWW25	5 38 41.60	−2 30 28.9	14.39	1.45	1	12.84	0.21	M3.5	31.01±0.51	<17.0	588±14	Y	Y	Y	Y	N	
S66	K1.01-114	5 39 36.06	−2 36 31.0	14.43	0.76	3	13.07	0.22	K7.0	48.55±0.63		56±23	N	N	N	N	N	
S67	p053841-0236	5 38 41.36	−2 36 44.5	14.49	1.46	3	12.99	0.22	M3.5	31.92±0.51	<17.0	577±14	Y	Y	Y	Y	Y	
S68	SWW86	5 38 40.54	−2 33 27.6	14.54	1.65	1	12.80	0.27	M4.0	31.79±0.73	<17.0	522±11	Y	Y	Y	Y	N	
S69	SWW31	5 38 39.03	−2 45 32.2	14.58	1.34	1	12.91	0.30	M2.5	30.67±0.56	<17.0	551±10	Y	Y	Y	Y	N	
S70	K1.02-91	5 38 56.23	−2 31 15.4	14.58	0.76	3	13.42	0.25	K7.0	69.74±0.63		37±9	N	N	N	N	N	
S71	SWW29	5 38 47.19	−2 34 36.8	14.64	1.45	1	12.56	0.48	M3.5	31.87±1.15	<17.0	306±9	Y	Y	Y	Y	N	
S72	J053834.5-024109	5 38 34.60	−2 41 08.8	14.72	1.46	1	13.10	0.33	M3.5	30.88±0.59	<17.0	547±3	Y	Y	Y	Y	N	
S73	SWW15	5 38 43.87	−2 37 06.8	14.80	1.79	1	12.84	0.37	M4.5	31.23±0.69	<17.0	453±7	Y	Y	Y	Y	N	
S74	SWW227	5 38 59.23	−2 33 51.4	14.83	1.26	1	12.89	0.58	M2.0	31.58±0.70	<17.0	395±33	Y	Y	Y	Y	Y	
S75	J053914.5-022834	5 39 14.47	−2 28 33.3	14.85	1.52	1	13.34	0.31	M3.5*	29.19±0.53	<17.0	61±6	Y	N	Y	Y	Y	
S76	K1.02-4	5 39 15.83	−2 36 50.7	14.86	1.50	3	13.25	0.32	M3.5	31.27±0.60	<17.0	579±14	Y	Y	Y	Y	Y	
S77	SWW230	5 38 42.86	−2 38 52.5	14.92	1.11	1	13.68	0.27	M1.0	41.98±0.50		70±6	N	N	N	N	N	
S78	SWW129	5 39 08.78	−2 31 11.5	14.97	1.63	1	13.04	0.45	M4.0	31.91±0.64	<17.0	470±13	Y	Y	Y	Y	N	
S79	K1.02-19	5 38 51.74	−2 36 03.3	14.97	1.87	3	12.91	0.26	M5.0	30.81±0.76	<17.0	524±10	Y	Y	Y	Y	Y	
S80	K3.01-167	5 38 49.70	−2 34 52.6	15.03	1.81	3	12.98	0.25	M4.5	31.15±0.80	<17.0	483±4	Y	Y	Y	Y	N	
S81	K8	5 38 50.78	−2 36 26.8	15.06	2.00	3	13.11	0.24	M5.0	31.09±1.51	$24.5^{+6.9}_{-2.1}$	442±37	Y	Y	Y	Y	N	
S82	K12	5 39 13.48	−2 23 51.9	15.18	1.41	3	13.95	0.24	M3.0	40.63±0.63		135±57	N	N	N	N	-	
S83	B3.01-67	5 38 46.85	−2 36 43.5	15.28	1.88	3	13.22	0.33	M5.0	30.22±1.39	$18.8^{+2.7}_{-1.4}$	502±3	Y	Y	Y	Y	N	
S84	SWW222	5 39 30.56	−2 38 27.0	15.30	1.32	3	13.81	0.22	M2.5	23.43±0.69		N	N	N	Y	N	Y	SB2
S85	K1.02-156	5 38 51.01	−2 27 45.7	15.51	1.00	3	14.28	0.23	M1.0	72.34±0.88		N	N	N	N	N	Y	SB2
S86	K3.01-263	5 38 28.25	−2 32 27.4	15.62	0.53	3	14.86	0.15	K3.5	113.37±1.07		43±13	N	N	N	N	Y	
S87	K4.03-422	5 38 45.28	−2 37 29.3	15.67	1.79	3	13.37	0.51	M4.5	30.19±0.91	<17.0	402±3	Y	Y	Y	Y	N	
S88	K3.01-226	5 38 35.29	−2 33 13.1	15.96	1.62	3	13.91	0.32	M4.0	31.03±0.98		582±7	Y	Y	Y	Y	N	
S89	r053808-0235b	5 38 08.66	−2 35 41.4	15.99	0.47	3	15.23	0.14	K2.0	16.54±2.02		N	N	N	N	N	N	SB2
S90	p053840-0232	5 38 40.89	−2 32 59.8	16.00	0.50	3	15.36	0.14	K3.0	62.12±1.50		64±6	N	N	N	N	N	
S91	p053902-0222	5 39 02.94	−2 22 41.8	16.02	1.36	3	14.79	0.17	M3.0	?		139±8	?	N	N	N	N	SB
S92	J053826.8-022846	5 38 26.84	−2 38 46.0	16.12	1.91	3	14.11	0.28	M5.0	30.66±0.94	<17.0	494±9	Y	Y	Y	Y	N	
S93	K1.02-18	5 38 42.39	−2 36 04.4	16.26	1.49	3	14.26	0.38	M3.5	29.66±1.26	<17.0	272±20	Y	Y	Y	Y	N	
S94	K4.03-1807	5 38 41.46	−2 35 52.3	16.32	2.25	3	14.00	0.37	M6.0	30.40±1.48	<17.0	322±27	Y	Y	Y	Y	N	
S95	2MJ05391483-0244415	5 39 14.83	−2 44 41.6	–	–	-	12.34	0.19	–	61.23±0.59		32±3	N	N	N	N	N	

Table 1. continued

ID	Name[a]	RA[b] (J2000)	DEC[b] (J2000)	I^c	$R-I^c$	ref[c]	J^b	$H-K_s^b$	SpT[d]	v_r (km/s)	$vsin(i)$ (km/s)	Li pEW[e] (mÅ)	Membership v_r	Li	Hα	Tot	X[f]	Notes
S96	K3.01-325	5 38 32.68	−2 31 15.6	–	–	-	12.55	0.08	–	−34.79±1.19		9±4	N	N	N	N	Y	SB1
S97	2MJ05391003-0242425	5 39 10.04	−2 42 42.5	–	–	-	12.97	0.24	–	78.96±0.68		70±6	N	N	N	N	N	
S98	2MJ05390458-0241493	5 39 04.59	−2 41 49.4	–	–	-	13.96	0.69	–	31.61±0.73	<17.0	443±57	Y	Y	Y	Y	N	

a: star names are from the following sources: 4771-..., r05..., p05... = Wolk (1996); SE = Scholz & Eislöffel (2004); SWW =Sherry et al. (2004); J05... = Zapatero Osorio et al. (2002); Béjar et al. (2004): note that we have dropped the S Ori prefix in front of the J05... names; K = Kenyon et al. (2005); B = Burningham et al. (2005); 2M = 2MASS catalogue.
b: coordinates and infrared photometry are from the 2MASS catalogue.
c: optical photometric data are taken from the following sources: (1) Sherry et al. (2004), (2) Wolk (1996), (3) Kenyon et al. (2005).
d: spectral types marked with asterisk have been derived spectroscopically by Zapatero Osorio et al. (2002). The other spectral types have been derived from photometry (see Sect. 2.1).
e: for double-lined spectroscopic binaries, we only indicate whether the line is identified (Y) or not (N)
f: Y = detected, N = undetected, - = outside the XMM field of view

Table 2. Photometry and membership for the observed sample stars in the λ Ori cluster.

ID	Name[a]	RA[b]	DEC[b]	I[c]	$R-I$[c]	ref[c]	J[b]	$H-K_s$[b]	SpT[d]	v_r	$vsin(i)$	Li pEW[e]	Membership				Notes
		(J2000)								(km/s)	(km/s)	(mÅ)	v_r	Li	Hα	Tot	
L01	LOri-003	5 35 55.43	9 56 30.9	12.65	0.74	2	11.42	0.21	K8.5	?		520±32	?	Y	Y	Y?	SB
L02	DM009	5 34 32.83	9 59 30.9	12.94	0.78	1	11.84	0.17	K4.5	27.09±0.26	$18.9^{+2.7}_{-1.9}$	464±23	Y	Y	Y	Y	
L03	LOri-016	5 35 13.46	9 55 25.3	13.18	0.89	2	11.96	0.23	K8.0	?		531±33	?	Y	Y	Y?	SB
L04	DM014	5 34 39.21	9 52 55.3	13.30	1.06	1	12.07	0.17	K7.0	27.72±0.18	<17.0	523±26	Y	Y	Y	Y	
L05	LOri-020	5 34 57.57	9 46 07.2	13.31	1.34	2	11.86	0.19	M2.0	21.43±0.53		18±29	N	N	Y	N	
L06	LOri-022	5 35 51.34	9 55 11.2	13.38	1.03	2	12.10	0.25	M1.5	28.40±0.38	<17.0	516±33	Y	Y	Y	Y	
L07	LOri-024	5 34 57.12	9 54 36.7	13.45	0.98	2	12.14	0.23	M0.0	27.28±0.29	<17.0	554±21	Y	Y	Y	Y	
L08	LOri-026	5 34 36.23	9 53 44.2	13.47	1.10	2	12.05	0.23	K9.5	27.29±0.43	$26.0^{+6.0}_{-1.0}$	581±43	Y	Y	Y	Y	
L09	DM019	5 34 48.46	9 57 15.7	13.73	1.20	1	12.42	0.18	M0.5	27.47±0.28	<17.0	571±27	Y	Y	Y	Y	
L10	LOri-030	5 35 12.54	9 55 19.5	13.74	1.21	2	12.43	0.26	M1.5	?		Y	?	Y	Y	Y?	SB2
L11	LOri-034	5 35 19.92	10 02 36.5	13.97	1.13	2	12.44	0.46	M1.0	24.36±0.30	<17.0	541±35	N	Y	Y	Y?	
L12	LOri-035	5 35 15.14	10 01 06.8	13.97	1.28	2	12.55	0.23	M2.5	21.36±0.72	$30.2^{+10.0}_{-6.2}$	572±21	N	Y	Y	Y?	
L13	LOri-036	5 34 39.29	10 01 28.7	13.98	1.49	2	12.58	0.23	M3.0	24.63±0.38		56±22	N	N	Y	N	
L14	LOri-037	5 34 35.61	9 59 43.3	13.99	1.18	2	12.46	0.24	M2.0	27.13±0.33	<17.0	566±57	Y	Y	Y	Y	
L15	LOri-040	5 35 39.48	9 50 32.8	14.06	1.32	2	12.55	0.29	M3.0	26.95±0.46	<21.3	561±45	Y	Y	Y	Y	
L16	LOri-041	5 35 30.45	9 50 34.1	14.10	1.45	2	12.50	0.27	M3.5	27.05±0.71	$61.9^{+11.8}_{-5.7}$	485±40	Y	Y	Y	Y	
L17	DM030	5 35 17.17	9 51 11.4	14.13	1.46	1	12.80	0.22	M1.0	27.30±0.27	<17.0	571±34	Y	Y	Y	Y	
L18	LOri-045	5 35 07.42	9 58 22.4	14.23	1.33	2	12.77	0.26	M2.0	26.89±0.42	<17.0	554±23	Y	Y	Y	Y	
L19	LOri-046	5 34 26.08	9 51 49.4	14.36	1.28	2	13.03	0.23	M2.0	−0.28±0.43		148±64	N	N	N	N	
L20	LOri-048	5 35 12.56	9 53 11.1	14.41	1.37	2	12.89	0.27	M2.5	27.04±0.44	<17.0	545±12	Y	Y	Y	Y	
L21	LOri-049	5 35 01.00	9 49 36.1	14.50	1.27	2	13.17	0.34	M2.0	24.06±0.36		64±13	N	N	N	N	
L22	LOri-050	5 34 56.40	9 55 04.6	14.54	1.36	2	12.88	0.29	M2.5	?		596±58	?	Y	Y	Y?	SB
L23	DM032	5 35 18.38	10 02 38.4	14.69	1.56	1	13.07	0.26	M1.5	26.98±0.34	<17.0	589±16	Y	Y	Y	Y	
L24	LOri-053	5 34 36.73	9 52 58.3	14.72	1.36	2	13.17	0.24	M2.5	27.00±0.42	<18.3	561±30	Y	Y	Y	Y	
L25	LOri-055	5 35 21.43	9 49 56.6	14.76	1.36	2	13.18	0.23	M2.5	26.70±0.39	<17.0	602±33	Y	Y	Y	Y	
L26	LOri-056	5 34 58.37	9 53 47.1	14.87	1.56	2	13.21	0.30	M3.0	26.84±0.56	<19.3	576±23	Y	Y	Y	Y	
L27	LOri-057	5 35 11.32	10 00 50.2	15.04	1.59	2	13.41	0.28	M3.5	26.99±0.49	<17.0	677±19	Y	Y	Y	Y	
L28	LOri-060	5 35 20.00	9 49 06.2	15.14	1.42	2	13.60	0.30	M2.5	27.22±0.45	<18.5	599±28	Y	Y	Y	Y	
L29	LOri-061	5 35 18.18	9 52 24.2	15.15	1.43	2	13.53	0.31	M2.5	26.80±0.47	$17.9^{+1.4}_{-1.8}$	591±30	Y	Y	Y	Y	
L30	LOri-062	5 35 15.33	9 48 37.0	15.16	1.46	2	13.63	0.28	M3.0	26.80±0.47	<17.0	648±48	Y	Y	Y	Y	
L31	LOri-068	5 34 48.02	9 43 26.2	15.20	1.56	2	13.52	0.27	M3.0	29.37±0.47	<17.0	698±25	N	Y	Y	Y?	
L32	LOri-069	5 34 43.97	9 48 35.6	15.20	1.69	2	13.38	0.34	M3.5	?		516±57	?	Y	Y	Y?	SB
L33	LOri-075	5 34 55.22	10 00 34.7	15.23	1.72	2	13.40	0.26	M5.0*	26.02±0.82	$61.3^{+11.5}_{-4.9}$	455±44	Y	Y	Y	Y	
L34	LOri-063	5 35 19.14	9 54 42.4	15.34	1.46	2	13.76	0.41	M3.0	27.19±0.47	<18.2	505±52	Y	Y	Y	Y	
L35	LOri-076	5 35 10.96	9 57 43.8	15.81	1.58	2	14.22	0.33	M3.0	27.52±0.50	<17.0	608±19	Y	Y	Y	Y	
L36	LOri-079	5 34 48.26	9 59 53.9	16.00	1.51	2	14.22	0.20	M3.0	27.03±0.51	<17.0	607±59	Y	Y	Y	Y	
L37	LOri-080	5 35 30.05	9 59 25.5	16.01	1.50	2	13.80	0.31	M3.0	25.74±0.81	$60.2^{+21.3}_{-5.9}$	523±20	Y	Y	Y	Y	
L38	LOri-083	5 35 43.41	9 54 26.8	16.02	1.54	2	14.27	0.26	M3.0	26.32±0.57	$19.1^{+7.9}_{-2.6}$	585±77	Y	Y	Y	Y	
L39	LOri-087	5 34 33.77	9 55 34.2	16.09	1.45	2	14.19	0.32	M4.5*	27.25±0.57	$18.4^{+6.0}_{-1.7}$	609±42	Y	Y	Y	Y	
L40	LOri-088	5 34 49.50	9 58 46.8	16.10	1.68	2	14.14	0.31	M3.5	26.75±0.53	<17.0	660±42	Y	Y	Y	Y	
L41	LOri-092	5 35 50.97	9 51 03.5	16.19	1.65	2	14.44	0.30	M3.5	26.66±0.57	$19.8^{+2.8}_{-2.6}$	661±53	Y	Y	Y	Y	
L42	LOri-093	5 34 41.20	9 50 16.3	16.21	1.61	2	14.46	0.24	M3.5	27.00±0.56	<18.3	623±61	Y	Y	Y	Y	
L43	LOri-094	5 34 43.17	10 01 59.8	16.28	1.75	2	14.40	0.37	M4.0	26.36±0.80	$54.8^{+5.5}_{-8.2}$	538±204	Y	Y	Y	Y	
L44	LOri-095	5 35 24.18	9 55 15.4	16.35	1.61	2	14.56	0.30	M6.0*	27.31±0.55	<19.7	559±30	Y	Y	Y	Y	
L45	LOri-096	5 35 11.13	9 57 19.6	16.37	1.65	2	14.63	0.33	M3.5	26.92±0.55	<19.1	553±48	Y	Y	Y	Y	
L46	LOri-100	5 35 00.10	9 46 14.0	16.43	1.65	2	14.77	0.22	M3.5	28.04±0.46	<17.0	717±43	Y	Y	Y	Y	
L47	LOri-102	5 35 22.02	9 52 52.3	16.50	1.74	2	14.63	0.27	M4.0	28.10±0.53	<17.0	584±62	Y	Y	Y	Y	

Table 2. continued.

ID	Name[a]	RA[b] DEC[b] (J2000)	I[c]	$R-I$[c]	ref[c]	J[b]	$H-K_s$[b]	SpT[d]	v_r (km/s)	$vsin(i)$ (km/s)	Li pEW[e] (mÅ)	Membership v_r	Li	Hα	Tot	Notes
L48	LOri-105	5 34 17.58 9 52 29.7	16.75	1.83	2	14.92	0.35	M4.0	26.45±0.70	<20.0	Y	Y	Y	Y	Y	
L49	LOri-106	5 35 28.77 9 54 10.2	16.76	1.72	2	14.78	0.42	M4.0	26.83±0.54	<17.0	636±132	Y	Y	Y	Y	

a: star names are from the following sources: DM = Dolan & Mathieu (1999); LOri = Barrado y Navascués et al. (2004).
b: coordinates and infrared photometry are from the 2MASS catalogue.
c: optical photometric data are taken from: (1) Dolan & Mathieu (1999), (2) Barrado y Navascués et al. (2004).
d: spectral types marked with asterisk have been derived spectroscopically by Barrado y Navascués et al. (2004). The other spectral types have been derived from photometry (see Sect. 2.1).
e: for the double-lined spectroscopic binary L10 and for the star L48, we only indicate whether the line is identified (Y) or not (N)

Table 4. Accretion properties of the σ Ori cluster members

ID	Hα pEW (Å)	Hα 10%width (km/s)	Log($\dot{M}_{acc}$) ($M_\odot$/yr)	NII 6583 Å (Å)	HeI 6678 Å (Å)	SII 6716 Å (Å)	SII 6731 Å (Å)	Disk class[a]
S02	-2.16± 0.14	146±12	-	≲0.05	≲0.05	≲0.05	≲0.05	III
S03	-1.39± 0.10	210±30	-	≲0.05	≲0.05	≲0.05	≲0.05	III
S04	-6.91± 0.14	-	-	≲0.10	≲0.10	≲0.10	≲0.10	III
S05	-31.93± 1.45	500±20	-8.0± 0.5	≲0.05	≲0.05	≲0.05	≲0.05	II
S06	-13.19± 1.38	504±57	-8.0± 0.7	0.14	≲0.03	≲0.03	≲0.03	EV[c]
S07	-0.94± 0.05	159±20	-	≲0.04	≲0.04	≲0.04	≲0.04	III
S10	-1.89± 0.21	216±39	-	≲0.05	≲0.05	≲0.05	≲0.05	III
S12	-5.93± 0.14	342±31	-9.6± 0.5	0.39	≲0.03	≲0.03	0.04	II
S13	-25.11± 0.72	539±20	-7.7± 0.5	0.07	≲0.06	≲0.06	0.10	II
S14	-40.03± 2.80	424±15	-8.8± 0.4	0.27	0.26	≲0.05	≲0.05	II
S15	-17.17± 0.80	226± 4	-10.7± 0.3	0.28	≲0.07	≲0.07	≲0.07	II
S16	-1.46± 0.17	169±36	-	≲0.03	≲0.03	≲0.03	≲0.03	III
S17	-17.14± 1.66	214±17	-10.8± 0.4	0.05	≲0.03	0.04	≲0.03	II
S18	-1.25± 0.05	143±27	-	≲0.03	≲0.03	≲0.03	≲0.03	III
S19	-2.45± 0.18	155±20	-	≲0.03	≲0.03	≲0.03	≲0.03	III
S21	-20.94± 1.20	317± 6	-9.8± 0.4	≲0.05	0.22	≲0.05	≲0.05	II
S23	-0.89± 0.13	338±88	-9.6± 0.9	0.05	≲0.05	≲0.05	≲0.05	II
S24	-3.59± 0.29	178±27	-	≲0.05	≲0.05	≲0.05	≲0.05	III
S26	-4.65± 0.13	-	-	≲0.03	≲0.03	≲0.03	≲0.03	III
S28	-5.60± 0.72	178±31	-	≲0.10	≲0.10	≲0.10	≲0.10	III
S29	-	-	-	-	-	-	-	EV
S32	-25.76± 0.79	422±15	-8.8± 0.4	0.66	0.35	0.06/0.08[b]	0.19/0.19[b]	I[d]
S33	-22.97± 0.49	445±23	-8.6± 0.5	≲0.08	0.11	≲0.08	≲0.08	II
S34	-10.19± 0.92	317±18	-9.8± 0.4	≲0.05	≲0.05	≲0.05	≲0.05	II
S35	-3.78± 0.14	141±24	-	≲0.09	≲0.09	≲0.09	≲0.09	III
S39	-5.02± 0.30	134±16	-	≲0.10	≲0.10	≲0.10	≲0.10	III
S41	-16.48± 0.76	191±10	< -11	2.34	0.19	1.06	1.57	EV[c]
S43	-27.43± 2.36	-	-	≲0.07	0.24	≲0.07	≲0.07	II
S44	-197.57±11.64	383± 4	-9.2± 0.4	1.14	0.14	≲0.08	≲0.08	II
S45	-6.71± 0.23	189±22	-	≲0.10	0.11	≲0.10	≲0.10	III
S47	-0.73± 0.02	237±14	-	≲0.05	≲0.05	≲0.05	≲0.05	III
S49	-4.73± 0.34	127±22	-	≲0.08	≲0.08	≲0.08	≲0.08	III
S51	-3.39± 0.22	157±12	< -11	≲0.05	≲0.05	≲0.05	≲0.05	EV
S52	-20.86± 1.68	251±14	-10.5± 0.4	≲0.10	0.24	≲0.10	≲0.10	II
S53	-	-	-	-	-	-	-	III
S55	-1.12± 0.08	93±18	-	≲0.03	≲0.03	≲0.03	≲0.03	III
S56	-3.89± 0.14	132±21	-	≲0.10	≲0.10	≲0.10	≲0.10	III
S57	-1.40± 0.17	125± 5	-	≲0.09	≲0.09	0.10	≲0.09	III
S58	-4.45± 0.27	116± 6	-	≲0.08	≲0.08	≲0.08	≲0.08	III
S59	-2.58± 0.04	89±13	-	≲0.10	≲0.10	≲0.10	≲0.10	III
S60	-3.98± 0.12	121±11	-	0.20	≲0.10	0.36	0.20	III
S62	-10.62± 0.57	237±17	-	0.10	≲0.03	0.09	0.04	III
S63	-14.11± 0.51	299±17	-10.0± 0.4	≲0.09	0.31	≲0.09	≲0.09	II
S64	-4.39± 0.10	102±12	-	≲0.08	≲0.08	≲0.08	≲0.08	III
S65	-4.35± 0.60	223±42	-10.7± 0.5	≲0.08	≲0.08	≲0.08	≲0.08	II
S67	-2.12± 0.05	114±19	-	≲0.08	≲0.08	≲0.08	≲0.08	III
S68	-8.79± 0.84	248±11	-10.5± 0.4	0.67	0.32	≲0.08	≲0.08	II
S69	-10.63± 0.65	379±14	-9.2± 0.4	0.13	0.22	0.25	0.12	II
S71	-113.26± 6.09	379± 5	-9.2± 0.4	6.48	0.57	0.44	1.24	II
S72	-3.80± 0.24	203±23	-10.9± 0.4	0.09	≲0.05	0.14	0.09	II
S73	-46.98± 3.86	207± 2	-10.9± 0.3	2.05	1.13	≲0.08	≲0.08	II
S74	-32.72± 1.70	372±13	-9.3± 0.4	0.54	0.98	0.21	0.55	II
S75	-4.60± 0.33	102± 9	-	≲0.10	≲0.10	≲0.10	≲0.10	III
S76	-4.75± 0.29	162±12	< -11	≲0.10	≲0.10	≲0.10	≲0.10	II
S78	-19.65± 0.19	401±26	-9.0± 0.5	≲0.10	0.50	≲0.10	≲0.10	EV[c]
S79	-15.87± 1.64	134± 9	-	≲0.08	0.21	0.14	≲0.08	III
S80	-5.76± 0.48	194± 6	< -11	≲0.08	0.17	≲0.08	≲0.08	II
S81	-8.18± 0.61	132±11	-	0.17	≲0.10	0.23	0.12	III
S83	-9.71± 1.30	132± 9	-	0.14	0.14	0.20	0.11	III

Table 4. continued

ID	Hα pEW (Å)	Hα 10%width (km/s)	Log($\dot{M}_{acc}$) ($M_\odot$/yr)	NII 6583 Å (Å)	HeI 6678 Å (Å)	SII 6716 Å (Å)	SII 6731 Å (Å)	Disk class[a]
S87	-36.32± 1.54	226± 4	-10.7± 0.3	4.07	0.18	0.41	0.49	II
S88	-7.16± 0.52	132±14	-	≲0.10	≲0.10	≲0.10	≲0.10	III
S92	-14.37± 0.49	157± 6	< -11	0.31	0.43	0.65	0.32	II
S93	-113.52± 6.42	70± 1	< -11	49.68	0.76	1.47	2.92	II
S94	-82.67±11.52	157± 3	< -11	6.34	1.03	0.30	0.62	II
S98	-16.14± 0.65	333± 2	-9.7± 0.4	0.14	0.14	0.12	0.06	II

a: disk clasification from Hernández et al. (2007): III=diskless, II=thick disk,
I= class I candidate, EV=evolved disk
b: splitted in two separate lines
c: classified as a transition disk candidate using the whole SED slope (see sec. 4.3 in Hernández et al. (2007))
d: classified as a class II using the whole SED slope (see sec. 4.3 in Hernández et al. (2007))

Table 5. Accretion properties of the λ Ori cluster members

ID	Hα pEW (Å)	Hα 10%width (km/s)	Log($\dot{M}_{acc}$) ($M_\odot$/yr)	NII 6583 Å (Å)	HeI 6678 Å (Å)	SII 6716 Å (Å)	SII 6731 Å (Å)	Disk class[a]
L01	-1.13±0.15	-	-	<0.04	<0.04	<0.04	<0.04	III
L02	-0.50±0.03	137±15	< -11	<0.03	<0.03	<0.03	<0.03	-
L03	-1.58±0.13	-	-	<0.03	<0.03	<0.03	<0.03	III
L04	-1.00±0.08	155±13	< -11	<0.03	<0.03	<0.03	<0.03	-
L06	-6.96±0.69	219±43	-	<0.03	0.12	<0.03	<0.03	III
L07	-2.00±0.12	137±20	-	<0.05	<0.05	<0.05	<0.05	III
L08	-5.30±0.30	198±18	-	<0.03	<0.03	<0.03	<0.03	III
L09	-2.44±0.23	155±22	< -11	<0.03	<0.03	<0.03	<0.03	-
L10	-	-	-	-	-	-	-	III
L11	-8.47±0.47	215±25	-10.80±0.40	<0.06	<0.06	<0.06	<0.06	II
L12	-3.32±0.35	146±34	-	<0.06	<0.06	<0.06	<0.06	III
L14	-3.67±0.34	148±29	-	<0.06	<0.06	<0.06	<0.06	III
L15	-5.15±0.62	141±18	-	<0.08	<0.08	<0.08	<0.08	III
L16	-7.05±0.86	306±52	-	<0.06	<0.06	<0.06	<0.06	III
L17	-1.89±0.15	132±50	< -11	<0.06	<0.06	<0.06	<0.06	-
L18	-3.04±0.33	123±27	-	<0.08	<0.08	<0.08	<0.08	III
L20	-3.34±0.44	159±36	< -11	<0.08	<0.08	<0.08	<0.08	EV
L22	-11.14±0.96	-	-	<0.09	<0.15	<0.09	<0.09	II
L23	-4.98±0.49	100±11	< -11	<0.09	<0.09	<0.09	<0.09	-
L24	-2.93±0.20	130±22	-	<0.09	<0.09	<0.09	<0.09	III
L25	-6.53±0.49	118±13	-	<0.09	<0.09	<0.09	<0.09	III
L26	-5.57±0.81	130±13	-	<0.10	0.15	<0.10	<0.10	III
L27	-5.20±0.52	107±11	-	<0.10	0.20	<0.10	<0.10	III
L28	-4.18±0.48	121±18	-	<0.08	<0.08	<0.08	<0.08	III
L29	-13.97±1.38	274±15	-10.20±0.30	<0.10	0.18	<0.10	<0.10	II
L30	-4.41±0.30	123±22	< -11	<0.10	<0.10	<0.10	<0.10	II
L31	-7.90±1.26	116±16	-	<0.10	<0.15	<0.10	<0.10	III
L32	-7.39±1.46	-	-	<0.10	<0.10	<0.10	<0.10	III
L33	-10.71±0.98	326± 9	-	<0.10	<0.10	<0.10	<0.10	III
L34	-19.14±2.53	230± 4	-10.70±0.30	3.60	0.80	0.26	0.31	II
L35	-4.92±0.60	121±20	-	<0.10	<0.10	<0.10	<0.10	III
L36	-5.06±0.53	127±25	< -11	<0.10	<0.20	<0.10	<0.10	EV
L37	-14.47±1.25	287±41	-10.10±0.50	0.10	<0.10	<0.10	<0.10	EV
L38	-5.32±0.68	134±16	-	<0.10	0.10	<0.10	<0.10	III
L39	-5.56±0.70	125±18	< -11	<0.10	<0.20	<0.10	<0.10	EV
L40	-9.44±1.12	107±13	-	<0.10	0.17	<0.10	<0.10	III
L41	-2.90±0.34	107±29	-	0.14	<0.10	<0.10	<0.10	III
L42	-6.25±0.94	137±29	-	<0.10	0.15	<0.10	<0.10	III
L43	-15.53±2.23	228±18	-	<0.20	<0.20	<0.20	<0.20	III
L44	-4.96±0.62	105± 9	-	<0.25	<0.25	<0.25	<0.25	III
L45	-6.97±1.10	114±20	< -11	0.22	<0.20	<0.20	<0.20	II
L46	-8.18±1.40	98± 6	-	0.60	<0.25	0.59	<0.25	III
L47	-5.94±0.96	93± 4	-	0.25	<0.10	0.25	0.16	III
L48	-	-	-	-	-	-	-	III
L49	-26.16±2.40	107± 4	< -11	0.70	0.40	0.40	0.30	II

a: disk classification from Barrado y Navascués et al. (2007): - =Spitzer non-members, III=diskless, II=thick disk, EV=evolved disk